



DEVELOPMENT OF AN ENERGY DEPENDENT
FINAL STATE DISTRIBUTION FOR T_2

MASTER THESIS

Technische Universität München

Cornelius Schätz

supervised by

Prof. Dr. Susanne MERTENS

January 18, 2019

Contents

| | | |
|----------|--|-----------|
| 1 | Theory of Neutrinos and sterile neutrinos | 4 |
| 1.1 | History of neutrino physics | 5 |
| 1.2 | Neutrino oscillations | 5 |
| 1.3 | Sterile neutrinos | 9 |
| 2 | The KATRIN experiment | 13 |
| 2.1 | Experimental setup | 13 |
| 2.1.1 | Tritium source | 14 |
| 2.1.2 | The Rear section | 15 |
| 2.1.3 | The Transport Section | 15 |
| 2.1.4 | The spectrometer section | 15 |
| 2.2 | The Detector Section | 16 |
| 2.3 | The TRISTAN Project | 16 |
| 3 | Development of an energy-dependent Final State Distribution | 20 |
| 3.1 | Introduction | 20 |
| 3.2 | The Sudden Approximation | 21 |
| 3.3 | Derivation of the transition probability | 24 |
| 3.3.1 | Evaluation of $T_{fi}^{(0)}$ | 25 |

| | | |
|-------|--|----|
| 3.3.2 | The zeroth order transition probability | 26 |
| 3.4 | The Born-Oppenheimer Approximation | 27 |
| 3.5 | B-Splines | 31 |
| 3.6 | Description of the FSD | 32 |
| 3.7 | Simplified model for an energy-dependent FSD | 33 |
| 3.7.1 | Energy-dependent groundstate | 33 |
| 3.7.2 | Energy-dependent excited FSD | 37 |

Abstract

In the search for dark matter, there arose many theoretical models over the course of the past centuries. One of those models includes the existence of a right-handed partner to the neutrino, the so called sterile neutrino. Its main property is, that it nearly doesn't interact with the active neutrino flavours or other Standard Model particles. There are many hypotheses, in which range the mass of such a sterile neutrino could be. With beta decay experiments like the KATRIN experiment, it could be possible, to detect the signature of a sterile neutrino in the energy spectrum of the electron. Since the KATRIN experiment is using molecular tritium, one tritium atom decays into a ^3He atom, whereas the other one remains. The new molecule, that arises, contains an orbital electron, whose eigenstates and eigenvalues change due to the decay. The energy of the orbital electron has a slight impact on the energy of the escaping beta electron and thus has to be respected. After the decay, the orbital electron can be in many excited states, each with a certain probability. The probability distribution of an orbital electron to end up in a certain excited state after the decay is called the Final States Distribution (FSD). The FSD has so far been calculated corresponding to beta electrons with an energy of 18.6 keV, allowing a more detailed analysis of the decay spectrum in the measurement of the neutrino mass. In order to look for a sterile neutrino with a keV mass, whose impact on the spectrum is far below the endpoint energy, the FSD needs to be known for different energies of the beta electron. The aim of this work is to develop a simplified model for this so called energy-dependent Final State Distribution. In the first chapter a short introduction to the physics of neutrinos and sterile neutrinos is given. In the second chapter, the experimental setup of the KATRIN experiment is described as well as the TRISTAN project, whose goal it is to redesign KATRIN in way, that it will be able to detect sterile neutrinos. In the third chapter, an introduction calculation of the FSD is given, followed by the development of a simplified model for the energy dependence of the groundstate FSD and of the first five excited states.

Chapter 1

Theory of Neutrinos and sterile neutrinos

Our understanding of neutrinos and the underlying physics has changed over the past few decades, still some of its most fundamental properties like the mass remain unknown. Another question that pops up when working on neutrinos is the existence of a right-handed partner. Understanding those properties is essential on the way to get a feeling for the origin of particle masses as well as for the role of primordial neutrinos and their influence on the evolution of large scale structures in the universe. A discovery of the right-handed partner of the neutrino with a mass in an keV range could unlock the secret nature of dark matter. This chapter shall give a short introduction to the theory of neutrinos and sterile neutrinos which will be a motivation for the following work. First, the history of the neutrino will be explained, going on to the theory of neutrino oscillations and their relation to a non-zero neutrino mass. The correlation between determining the mass of the neutrino and β decay experiments will be explained. After that, the concept of sterile neutrinos, which are the right-handed partners of the neutrinos, will be described. Their role as a possible dark matter candidate and their correlation to the β decay energy spectrum will be explained.

1.1 History of neutrino physics

The first time, the idea of the neutrino was postulated was in the year 1930 by Wolfgang Pauli [13]. Trying to describe the continuous energy spectrum of the electron in a β decay process, he assumed the existence of a new particle, which he then called a neutron. In his hypothesis, this particle was staying in the nucleus, having no electrical charge and a spin $\frac{1}{2}$. As two years later the "real" neutron was discovered by Chadwick, being a neutral particle with a mass just slightly higher than the proton's mass, Pauli changed the name of his particle to neutrino. Shortly after the discovery of the neutron, Fermi formulated the first quantum theoretical theory of β decays [14]. In this model, a massive neutral particle, being the neutron, decays into a proton, an electron and into a neutral, massless particle, called the neutrino ν , or to be more precise, into an anti-electron neutrino $\bar{\nu}_e$.

$$n \rightarrow p + e + \bar{\nu}_e \quad (1.1)$$

In 1956, Cowan [15] discovered the existence of the inverse β decay.

$$p + \bar{\nu}_e \rightarrow n + e^+ \quad (1.2)$$

In this process a proton and an anti-electron neutrino decay into a positron and a neutron. After the detection of a muon flavoured neutrino in 1962, the idea came up, that neutrinos, similarly to the leptons, occur in different flavours. The last neutrino flavour, called a tauon neutrino, was only discovered 20 years later, after remaining theoretical for a long time.

1.2 Neutrino oscillations

Neutrino oscillations were first predicted by B. Pontecorvo [16]. The first experimental evidence was given about ten years later by experiments such as Homestake, SNO and Kamiokande. In the Homestake experiment the flux of solar electron neutrinos was measured. A high deficit of high energy neutrinos compared to the solar neutrino model was detected, often recalled as the solar neutrino problem. The solution to that are the so-called neutrino oscillations. In this model, a neutrino of flavour x can turn with a certain probability into a neutrino with flavour y .

Mathematically, neutrino oscillations are explained using the PNMS (Pontecorvo-Magi-Nakagawa-Sakata) matrix U_{li} :

$$\nu_l = \sum_{i=1}^3 U_{li} \nu_i \quad (1.3)$$

with the index l indicating the flavour eigenstates of the neutrino (e, μ, τ) and i indicating the mass eigenstates. The equation in a written out form looks like:

$$\begin{pmatrix} \nu_e \\ \nu_\mu \\ \nu_\tau \end{pmatrix} = \begin{pmatrix} U_{e1} & U_{e2} & U_{e3} \\ U_{\mu1} & U_{\mu2} & U_{\mu3} \\ U_{\tau1} & U_{\tau2} & U_{\tau3} \end{pmatrix} \begin{pmatrix} \nu_1 \\ \nu_2 \\ \nu_3 \end{pmatrix}$$

In a simplified model of neutrino oscillations with only two flavour and mass eigenstates, the probability of a x flavoured neutrino oscillating into a y flavoured one would be:

$$P(\nu_x \rightarrow \nu_y) = \sin^2(2\theta) \cdot \sin^2 \left(1.27 \cdot \Delta m_{xy}^2 / eV^2 \frac{L/km}{E_\nu/GeV} \right) \quad (1.4)$$

E_ν denotes the energy of the neutrino, $\Delta m_{xy}^2 = m_x^2 - m_y^2$ is the difference of the squared mass corresponding to the mass eigenstates and L is the distance the neutrino traveled. The variable θ stands for the mixing angle between the flavour eigenstates. Since the oscillation probability is dependent on the squared mass difference, one can deduce, that neutrino oscillations imply a non-zero mass of this particle.

Determining the neutrino mass is an aim of many experiments in the area of experimental neutrino research. Such experiments are divided into the kinematics of the escaping electron in β decay, half-life measurements in the neutrinoless double β decay ($0\nu\beta\beta$) and cosmological observations. Analyzing the energy spectrum of the electron in an nuclear β decay would directly yield the neutrino mass as an observable whereas other approaches like the cosmological observations indirectly measure the sum of all neutrino mass eigenstates and depend strongly on the used cosmological model.

In β decay, a neutron decays into a proton, emitting a W^- boson, which then decays into an electron and an anti-electron neutrino. The derivation of the differential spectrum of the tritium beta decay will be now explained shortly following [17]. Using Fermis Golden Rule, the decay rate is given by

$$\Gamma = 2\pi \sum \int |M|^2 df \quad (1.5)$$

with M being the transition matrix element and $\sum \int df$ representing the sum (integral) over all possible discrete (continuous) final states f . First focus on the term df . Let dn be the number of different final states of outgoing particles inside a volume V into the solid angle $d\Omega$ with momentum $[p, p + dp]$. One then can write

$$dn = \frac{V d^3\vec{p}}{h^3} = \frac{V p^2 dp d\Omega}{h^3} \quad (1.6)$$

Using the relation $E_{tot}^2 = m^2 + p^2$ which implies $p dp = E_{tot} dE_{tot}$, this expression can be written as:

$$dn = \frac{V p E_{tot} dE_{tot} d\Omega}{(2\pi)^3} \quad (1.7)$$

The density of states in a certain energy interval and solid angle becomes:

$$\frac{dn}{dE_{tot} d\Omega} = \frac{V p E_{tot}}{(2\pi)^3} \quad (1.8)$$

Since the mass of the daughter nucleus is much higher than the energies of the two emitted leptons, it is a valid assumption to say that the nucleus does not have any kinetic energy at all. The density of states for the electron and the neutrino becomes

$$\rho(E_e, E_\nu d\Omega_e, d\Omega_\nu) = \frac{V^2 \sqrt{E_e^2 - m_e^2} E_e \sqrt{E_\nu^2 - m_\nu^2} E_\nu}{(2\pi)^6} \quad (1.9)$$

Let's now focus on the matrix element M . This can be divided into a leptonic and a nuclear part:

$$M = G_F \cos\theta_C M_{lep} M_{nuc} \quad (1.10)$$

with θ_C denoting the Cabibbo angle. Since the decay of tritium is either a allowed or superallowed transition, means a decay in which none of the leptons has any angular momentum and both are treated as plane waves, the leptonic matrix element becomes:

$$|M_{lep}|^2 = \frac{1}{V^2} F(E, Z') \quad (1.11)$$

$F(E, Z')$ is denoting the Fermi function, which describes the Coulomb interaction of the beta electron and the daughter nucleus having an atomic number Z' . In an allowed or superallowed transition the nuclear matrix element is not dependent on the energy of the escaping electron. It can thus be divided into a Fermi part (with the nuclear spin difference being zero) and a Gamov-Teller part (with a nuclear spin

difference being either zero or ± 1). What remains, is an angular correlation of the two outgoing leptons. The directions of the leptons are connected to each other via the factor:

$$1 + a(\vec{\beta}_e \cdot \vec{\beta}_\nu) \quad (1.12)$$

with $\beta_i = v_i/c$ and a being 1 for pure Fermi transitions and $-1/3$ for pure Gamov-Teller transitions according to [18]. With this knowledge it is possible to compute the partial decay rate Γ_0 with P_0 being the probability of this very decay channel:

$$\Gamma_0 = 2\pi P_0 \int_{E_e, E_\nu, \Omega_e, \Omega_\nu} |G_F \cos\theta_C M_{lep} M_{nuc}|^2 dn_e dn_\nu = \quad (1.13)$$

$$\frac{P_0}{(2\pi)^5} \int_{E_e, E_\nu, \Omega_e, \Omega_\nu} G_F^2 \cos^2\theta_C F(E, Z') |M_{nuc}|^2 \cdot \quad (1.14)$$

$$\sqrt{E_e^2 - m_e^2} E_e \sqrt{E_\nu^2 - m_\nu^2} E_\nu (1 + a\vec{\beta}_e \vec{\beta}_\nu) \cdot \quad (1.15)$$

$$\delta(Q - (E_e - m_e) - E_\nu - E_{rec}) dE_e d\Omega_e dE_\nu d\Omega_\nu \quad (1.16)$$

Q stands for the energy released in the decay process. This energy is, according to the δ function, distributed into the kinetic energy of the electron, the total energy of the neutrino and the recoil energy of the daughter nucleus. What we are now actually interested in, is a formula for the differential energy spectrum of the escaping electron

$$\frac{dN}{dt dE} = \frac{d\Gamma}{dE} \quad (1.17)$$

which gives the number of counts per time and energy unit. The differential decay spectrum takes the following form:

$$\frac{d\Gamma}{dE} = C \cdot F(E, Z') \cdot p_e \cdot (E + m_e) \cdot \sqrt{(E + m_e)^2 - m_e^2} \cdot \quad (1.18)$$

$$(E_0 - E) \cdot \sqrt{(E_0 - E)^2 - m_\beta^2} \quad (1.19)$$

The constant C stands for the fraction $\frac{G_F^2 \cos^2\theta_C |M_{nuc}|^2}{2\pi^3}$. m_β is the effective neutrino mass, respectively

$$m_\beta^2 = \sum_i |U_{ei}|^2 m_i^2 \quad (1.20)$$

summing over all flavours. Noting that in the decay process of a tritium atom bound in a T_2 molecule there is a orbital electron, which can be in several excited states

with energy E_f and probability P_f , the differential decay rate changes to:

$$\frac{d\Gamma}{dE} = \sum_f P_f \cdot C \cdot F(Z, E) \cdot p \cdot E_{tot} \cdot (E_0 - E - E_f) \cdot \sqrt{\Theta(E_0 - E - E_f - m_\nu) \cdot ((E_0 - E - E_f)^2 - m_\nu^2)} \quad (1.21)$$

Measuring the electron energy spectrum will yield the total decay energy minus the energy of the anti-electron neutrino. Thus, the spectrum of the electron is shifted by the effective mass of the neutrino

$$m_{\bar{\nu}_e} = \sqrt{\sum_{i=1}^3 |U_{ei}|^2 M_{\nu i}^2} \quad (1.22)$$

In the approach of measuring the neutrino mass using the neutrinoless double beta decay, one takes a look at the process of two neutrons decaying into two protons, two electrons and two anti-electron neutrinos. The continuous energy spectrum of the electron is shifted by two times the neutrino mass. If the neutrino is a Majorana fermion, meaning it is its own anti-particle, then the anti-electron neutrino might be directly absorbed in the second beta decay inside the nucleus. The emitted electrons would result in a mono-energetic line at the endpoint of the spectrum, with decay rate of the neutrinoless double beta decay being proportional to the effective Majorana mass $m_{\beta\beta}$.

In cosmological observations, like done by WMAP and the Planck Satellite. data from cosmic microwave background and baryonic acoustic oscillations were combined based on the Λ CDM model.

1.3 Sterile neutrinos

A natural extension of the Standard Model of particle physics (SM) would be the introduction of a right-handed neutrino, which from now on will be called sterile neutrinos. Those neutrinos are only sensitive to gravitational interaction. Sterile neutrinos make up a fourth mass eigenstate ν_4 with eigenvalue m_4 and mix up with the other neutrino flavours. There are three possible models, which mass the sterile neutrino could have. Those are considering sterile neutrinos in the mass range of eV, keV and GeV. Sterile neutrinos with an electron-Volt mass could explain certain anomalies occurring in reactor experiments for example. If the sterile neutrino has

a mass in the range of kilo electron volts, they could be a viable candidate for dark matter. Giga electron volt sterile neutrinos could explain the small masses of the interacting neutrinos via the see-saw mechanism as well as being a solution for baryogenesis (the asymmetry between matter and anti-matter in our universe). Since the aim of this work is to develop a model to possibly find keV sterile neutrinos, only these will be explained in some detail. Sterile neutrinos with a mass in the keV range would serve as warm dark matter, a scenario between cold and hot dark matter. The parameters of interest are its mass eigenvalue m_4 as well as the active-sterile mixing amplitude $\sin^2\theta_s$. The main effort of cosmological observations is to constrain the allowed region of these two free parameters. One can already guess, that the mixing amplitude is very small, since sterile neutrinos are not supposed to interact a lot with the other neutrino flavours. In the search for the mass of sterile neutrinos, the beta decay of tritium is with its endpoint energy of $E_0 = 18.6keV$ a perfect tool to probe the impact of an (still hypothetical) sterile neutrino. The mixing of the four neutrino flavours is described with an extended PMNS matrix:

$$\begin{pmatrix} \nu_e \\ \nu_\mu \\ \nu_\tau \\ \nu_s \end{pmatrix} = \begin{pmatrix} U_{e1}^* & U_{e2}^* & U_{e3}^* & U_{e4}^* \\ U_{\mu1}^* & U_{\mu2}^* & U_{\mu3}^* & U_{\mu4}^* \\ U_{\tau1}^* & U_{\tau2}^* & U_{\tau3}^* & U_{\tau4}^* \\ U_{s1}^* & U_{s2}^* & U_{s3}^* & U_{s4}^* \end{pmatrix} \begin{pmatrix} \nu_1 \\ \nu_2 \\ \nu_3 \\ \nu_4 \end{pmatrix}$$

One can then write

$$1 = \sum_{i=1}^3 |U_{ei}^2| + |U_{e4}| := \cos^2\theta_s + \sin^2\theta_s \quad (1.23)$$

with θ_s denoting the active-sterile mixing angle. It can be considered as an effective mixing of an active neutrino with mass m_{light} and sterile neutrino with mass m_4 , since it is not possible yet to resolve the light mass states. Having a look at the differential decay rate corresponding to the beta decay of tritium together with an influence of a sterile neutrino, it looks like:

$$\frac{d\Gamma}{dE} = \cos^2\theta_s \frac{d\Gamma}{dE}(m_{light}^2) + \sin^2\theta_s \frac{d\Gamma}{dE}(m_4^2) \quad (1.24)$$

with

$$\frac{d\Gamma}{dE}(m_4^2) = C \cdot F(E, Z') \cdot p_e(E + m_e) \sqrt{(E + m_e)^2 - m_e^2} (E_0 - E) \sqrt{(E_0 - E)^2 - m_4^2} \quad (1.25)$$

The spectrum of a decay into a sterile neutrino (equation above) would have a lower endpoint, to be precise $E_0 - m_4$ and a really small amplitude $\sin^2\theta_s$. Thus,

the impact of a sterile neutrino on the whole beta spectrum results in a kink-like signature at $E_0 - m_4$ and a tiny distortion of the amplitude in the region between zero energy and $E_0 - m_4$. This kink-like signature can be seen in Figure 1.1. A mass of 10 keV and a mixing angle of 27 degrees has been used. Although the mixing angle is extremely unrealistic, this example shows quite well the imprint of a sterile neutrino on the spectrum of the beta electron.

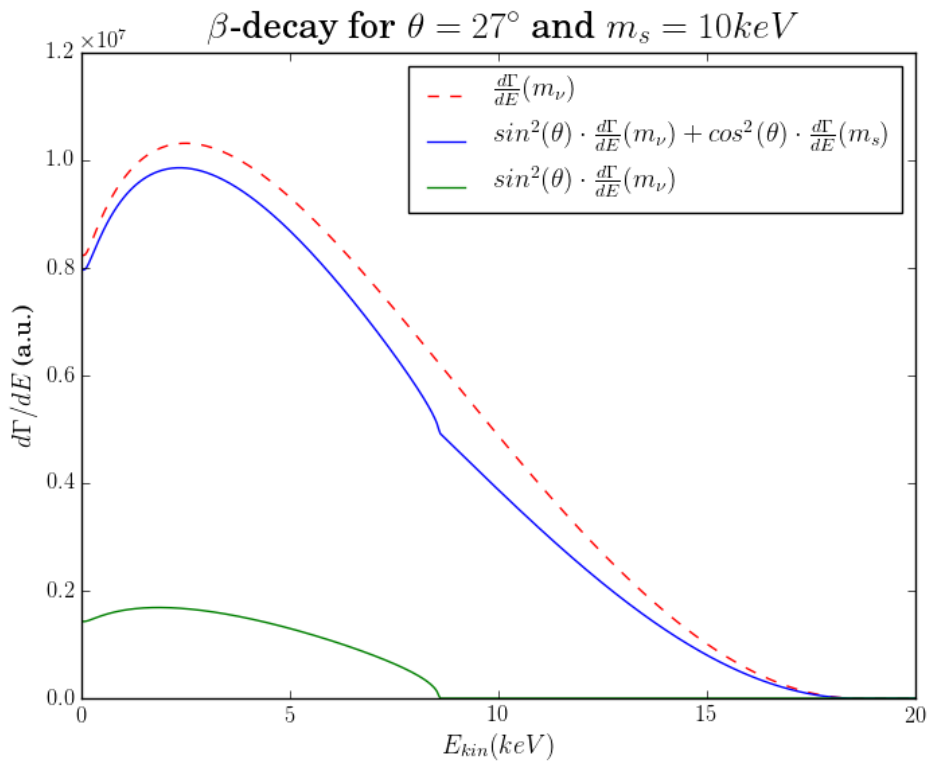


Figure 1.1: Differential decay rate for the beta decay of tritium without sterile neutrinos (red dashed) and with an sterile neutrino having a mass of 10 keV and a mixing angle of 27 degrees (which is unrealistic, but shows quite well the imprint of an sterile neutrino on the energy spectrum of the escaping electron)

Since tritium in reality occurs in molecular form, for example as a T_2 molecule, the energy of the remaining orbital electron needs to be subtracted from the energy of the escaping electron, when having a look at the differential decay rate. This has a slight impact on the spectrum. The aim of this work will be to develop a simplified

model for the behaviour of the orbital electron after the decay in order to analyze the spectrum more detailed.

Chapter 2

The KATRIN experiment

The Karlsruhe TRitium Neutrino experiment (KATRIN) is a beta decay experiment with the goal to measure the effective mass of the anti-electron neutrino. This happens with the use of high precision spectroscopy of the beta electrons produced in the decay with an energy close to the endpoint E_0 . This chapter shall give a short introduction to the measurement principle of KATRIN and to the experimental setup.

2.1 Experimental setup

With the aim to detect tiny distortions of the tritium spectrum near the endpoint due to a non-zero effective neutrino mass, the KATRIN experiment implements a high countrate of a stable molecular tritium source combined with a changeable retarding potential acting as a high pass filter. The integral spectrum ($\Gamma(t) = \frac{dN(t)}{dt}$) is determined measuring the count rates at different retarding potentials. The main components of the experimental setup will be described in the following and can be seen in Figure 2.1. To the very left, there is the Rear Section, connected to the Tritium Source (WGTS). To the right of the WGTS is the Transport Section, followed by the Spectrometer Section. At the right end of the whole experimental setup, there is the Detector Section. More detailed information on this topic may be found in [19].

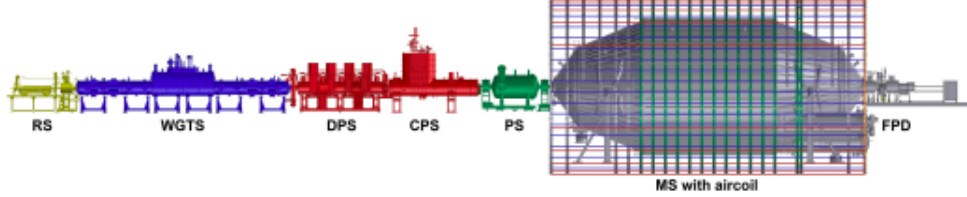


Figure 2.1: The whole KATRIN experiment seen from a side view with a length of 70m. At the very left, there is the rear section, connected to the Windowless Gaseous Tritium Source (WGTS). To the right of the WGTS is the Transport Section (DPS and CPS), followed by the Spectrometer Section (PS+ Main Spectrometer) and in the end the Detector Section (FPD).

2.1.1 Tritium source

In the KATRIN experiment, the used emitter of beta electrons is tritium, in its molecular form T_2 , one of the isotopes of hydrogen. The decay process is the following:



There are some reasons, why molecular tritium is used for this experiment. First, it has a pretty low endpoint energy of $E_0 = 18.6keV$. Although the total number of counts per second increases with energy, it drops near the endpoint proportional to E^{-3} . Therefore a low endpoint energy is preferred [20]. Since the decay of tritium is a superallowed transition between mirror nuclei, it has a relatively short half life of about 12.3 years. This implied high statistics with low source density during the lifetime of the experiment [20]. Another important reason is, that the molecular structure of tritium is, compared to the structure of molecules including heavier atoms, is less complicated. Thus the calculations of atomic effects can be done more accurately. In KATRIN, the tritium is injected at the center into a 10m long tube, which is called the Windowless Gaseous Tritium Source (WGTS). The molecules diffuse towards both ends of the WGTS are pumped out at both ends using turbo-molecular pumps. The pumped out tritium gets collected, reinjected and thus forming a closed tritium cycle. Including the two pumping sections, the WGTS is 16 m long. The WGTS beam tube is situated in a almost homogenous magnetic field of 3.6T. The direction of the field shows into the direction of the beam, guiding the electrons from the decay towards the spectrometer. The WGTS tube itself is made of stainless steel and has a diameter of 90 mm. It is kept at a low

temperature of 27 K, which makes sure that the column density $\rho d = 5 \cdot 10^{17} \text{cm}^{-2}$. The main systematics of the Windowless Gaseous Tritium Source are due to the stability of the column density, which is highly dependent on the pressure of the injection and the temperature. Thus the temperature has to be kept stable with a very high precision. This is done using a two phase NEON cooling system resulting in temperature variations smaller than 30mK . With the above given column density, the WGTS ensures an activity of the source of 10^{11} counts per second.

2.1.2 The Rear section

From the beta electrons escaping the tritium molecules at least half of them will leave the WGTS in a backwards direction. This is due to the fact, that the starting polar angle of all the electrons is uniformly distributed. Additionally, most of the electrons going in forward direction will be either reflected at a magnetic field larger than the field of the source or at the analyzing plane. This means, that nearly all electrons resulting from the beta decay of tritium will hit the rear wall. Its task is, to monitor the activity of the tritium.

2.1.3 The Transport Section

The Transport or Pumping Section, is divided into two subsections - the Differential Pumping Section (DPS) and the Cryogenic Pumping Section (CPS). The flow of the tritium from the source to the Spectrometer section is reduced by those two sections by a 14 orders of magnitude. The DPS is equipped with Turbo Molecular Pumps, reducing the tritium flow by five orders of magnitude. To prevent positive ions from entering the Main Spectrometer, the WGTS and the DPS are byased with a negative voltage. In the CPS, the tritium molecules are trapped by cryo-sorption at 6K. The CPS is designed such that the probability of tritium molecules hitting the vessel walls gets increased.

2.1.4 The spectrometer section

The KATRIN experiment has in total three spectrometers. First, there is the Monitor Spectrometer [21], which is used to keep track of the Main Spectrometer's high voltage system. Then there is the Pre Spectrometer [22] as a retention system for

low energy electrons and last the Main spectrometer [19]. The Main spectrometer is used as an energy filter for the electrons working with high precision. The Main Spectrometer is a Magnetic Adiabatic Collimation Filter combined with an Electrostatic Filter (short MAC-E Filter). In Figure 2.2 it is shown how it works. The gradient of the magnetic field collimates the momenta of the electrons in axial direction. The electric field's task is to reflect electrons with a kinetic energy lower than the energy of the electric field qU , q denoting the charge and U the voltage of the high voltage system. The energy resolution of the MAC-E filter is:

$$\frac{\Delta E}{E_e} = \frac{B_a}{B_p} = \frac{3 \cdot 10^{-4} T}{6 T} \quad (2.2)$$

B_s is denoting the magnetic field in the analyzing plane whereas B_p is the maximal magnetic field generated by the pinch magnets. For energies of the electron around the endpoint of the spectrum $E_e = 18.6 \text{ keV}$ the Main spectrometer gives a resolution of $\Delta E = 0.93 \text{ eV}$.

2.2 The Detector Section

The Detector Section is set up at the end of the whole experimental setup. A schematic overview of how it is built can be seen in Figure 2.3. It encompasses the silicon based pin-diode detector, or Focal Plane Detector (FPD) and a post acceleration electrode. The FPD has a radius of 4.5 m and is divided into 148 pixels. Each pixel has an area of 44 mm^2 . If an electron passed the potential of the Main Spectrometer, it is then detected in the FPD. Scanning the energy spectrum of the electron using different potentials in the Main Spectrometer allows to count electrons with an energy higher than the potential in the Main Spectrometer. Thus it is possible to measure an integral energy spectrum of the beta decay.

2.3 The TRISTAN Project

The TRISTAN group at the KATRIN experiment, with TRISTAN being short for TRitium Investigation of STerile to Active Neutrino mixing, aims to realize a technical solution for the search of keV sterile neutrinos with KATRIN. It allows to investigate a mass range of the sterile mass eigenstate m_4 in a range between 0 keV

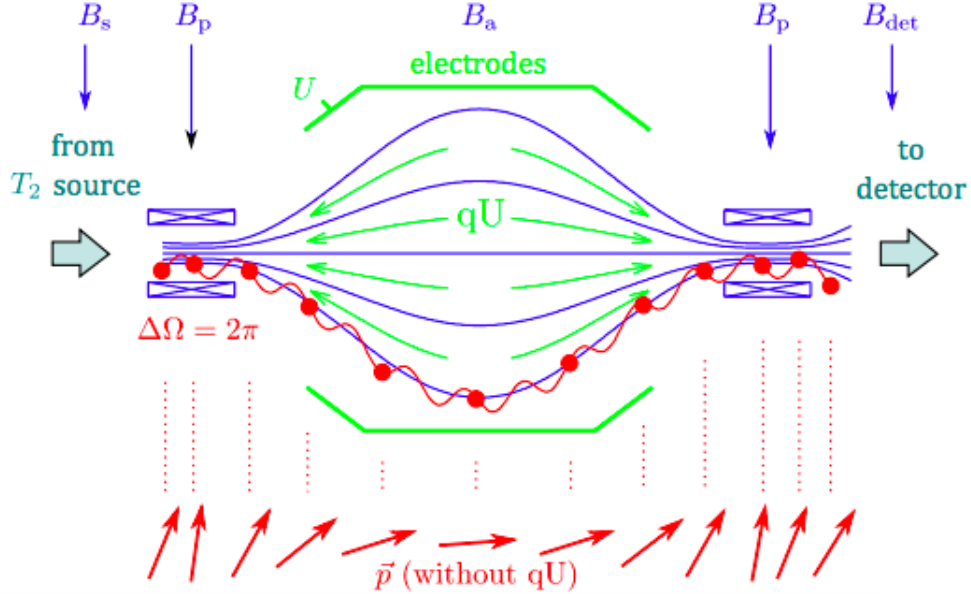


Figure 2.2: The working principle of the MAC-E Filter used in the KATRIN experiment. Electrons, that get into the spectrometer, are guided along the magnetic field lines into the middle of the Main Spectrometer, referred to as the analyzing plane. In the middle of the Main Spectrometer the electrostatic potential has its maximum, such that only electrons with high enough axial momenta are able to get to the detector.

and 18.6 keV [23]. Since this requires a measurement of the total beta decay energy spectrum, the electron rate at the detector needs to be increased by a factor of 10^8 . The TRISTAN group considers a two-stage approach. In the first stage, the Pre-KATRIN stage, the aim is to improve current laboratory limits after some days of measurements. To allow the measuring of the whole beta-spectrum, the spectrometer's potential needs to be lower than 1kV. Additionally, the source of the tritium source needs to be reduced by a factor of 10^5 , due to the fact that the FPD only allows a count rate of 100 kilo counts per second. In the Post-KATRIN stage, the aim is to measure mixing angles below $\sin^2\theta = 10^{-6}$. Therefore, the whole strength of the source is needed. This implies a major modification of the experimental setup at KATRIN, especially in the Detector section, where a detector is required which will be able to handle the full rate of incoming electrons. There currently is work going on concerning the development of a Post-KATRIN detector. The TRISTAN group

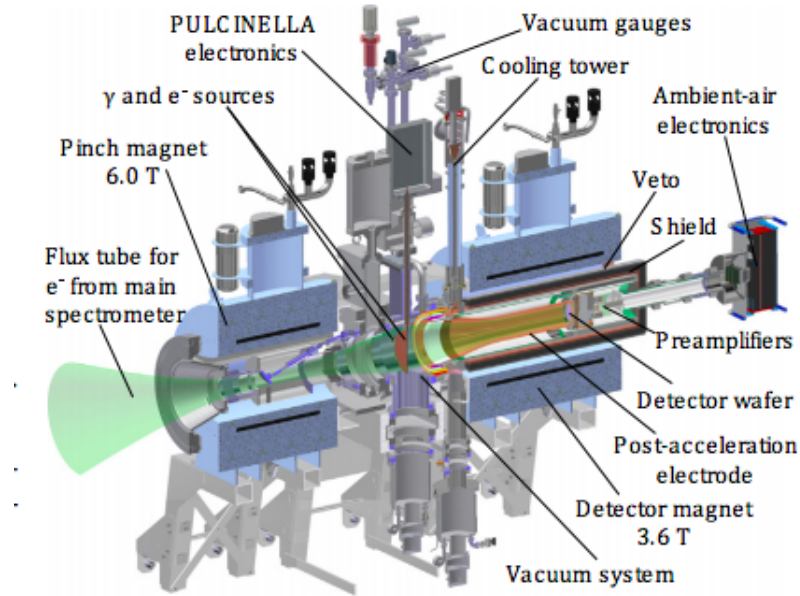


Figure 2.3: Schematic overview of the Detector Section set up at the end of KA-TRIN's experimental setup. The Main Spectrometer is on the left side of the shown setup.

collaborates with the HalbLeiter LaborMunich (HLL) and the Lawrence Berkeley National Laboratory (LBNL), working on a prototype of a new pn-type silicon drift detector [24]. Each of those prototype detectors consists of seven hexagonal pixels. Each of these pixels has a small read-out contact in the center. Several drift rings are positioned around the read-out contact. A picture of the detector prototypes can be seen in Figure 2.4.

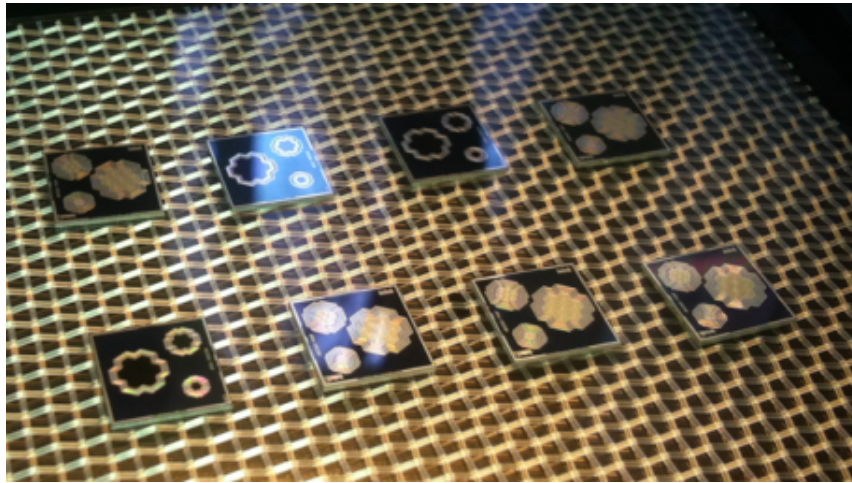


Figure 2.4: Picture of the detector prototypes for the TRISTAN project produced at the HLL. Each chip contains seven pixels. The designs differ in size and the number of drift rings.

Chapter 3

Development of an energy-dependent Final State Distribution

3.1 Introduction

As described in chapter one regarding the physics of active and sterile neutrinos, in the search for sterile neutrinos using experiments based on the nuclear β decay of tritium molecules (or isotopologes) the whole spectrum needs to be analysed, not only the endpoint, as in the measurement of the neutrino mass. The differential decay rate of the spectrum is given by

$$\frac{d\Gamma}{dE} = \sum_f P_f \cdot C \cdot F(Z, E) \cdot p \cdot E_{tot} \cdot (E_0 - E - E_f) \cdot \sqrt{\Theta(E_0 - E - E_f - m_\nu) \cdot ((E_0 - E - E_f)^2 - m_\nu^2)} \quad (3.1)$$

with E_f being the energy of the remaining orbital electron in the daughter molecule and P_f the corresponding probability, that the orbital electron will end up in this state after the decay. The probability distribution for each state, that the electron can have in the daughter molecule, is called the Final State Distribution (FSD). So far, the FSD has only been calculated for the case of the β electrons having an energy of 18.6 keV, thus for analysing the endpoint of the spectrum. Since the impact of

sterile neutrinos on the spectrum is way beyond the endpoint, an energy-dependent FSD is needed. The aim of this work is, to develop a simplified model describing the behaviour of the FSD for β energies below the endpoint, down to 12 keV β electrons. First, the theoretical background needed to develop that model will be discussed. The theoretical calculations are based on the Sudden approximation, used to handle the evaluation of the matrix element. The derivation of the matrix element will be done by the Lippmann Schwinger ansatz [4], ending up in a zeroth order transition matrix element, that is independent on the recoil momentum of the escaping beta electron. The initial and final state in the matrix element are the wavefunctions of the T_2 molecule and the daughter molecule ${}^3HeT^+$. To get them, the Schrödinger equation needs to be solved. Therefore the Born-Oppenheimer approximation is used, to separate the molecular Schrödinger equation into a electronic and a nuclear part. Solving the nuclear part of the coupled equations requires numerical methods. Therefore the technique of expanding wavefunctions in terms of B-Splines will be explained. Following the theoretical framework, a description of the four main parts of the FSD will be given. After that, the focus will lie on the development of an simplified energy-dependent description of the first two parts - the groundstate and the first five electronically excited states. In the conclusion we will have a look at the differences to the use of old models in the beta decay spectrum containing sterile neutrinos.

3.2 The Sudden Approximation

To get the Final State Probability distribution, the transition probabilities from an initial state (in this case the T_2 molecule) to a final state (HeT^+) need to be calculated. Since the calculations of the matrix elements can get pretty complicated, the first step is to simplify those using the so called Sudden approximation [9]. Quantum mechanical systems are in general described by a Hamiltonian H . If this system goes through a change (i.e. a nuclear β decay), the Hamiltonian changes as well as the properties of the system. To treat this change in a simplified manner, the sudden approximation is applied. Start with a Hamiltonian H_0 describing a quantum mechanical system, before a sudden perturbation to the system happens at time $t = 0$ to a system described by the Hamiltonian H_1 . Both Hamiltonians are assumed to be independent of time. Before the change, for $t < 0$, the Schrödinger equation for the system is:

$$H_0\psi_k = E_k^{(0)}\psi_k \quad (3.2)$$

with $E_k^{(0)}$ and ψ_k being the eigenvalues and eigenfunctions of the Hamiltonian H_0 . The eigenfunctions of this system are assumed to form a complete, orthonormal set ψ_k . The solution to the time-dependent Schrödinger equation

$$i\hbar \frac{\partial}{\partial t} \psi_k = H_0 \psi_k \quad (3.3)$$

is then described by the expansion

$$\psi(t) = \sum_k a_k \psi_k e^{-iE_k^{(0)}t/\hbar} \quad (3.4)$$

The summation goes through all eigenfunctions from the complete and orthonormal set ψ_k . The coefficients a_k shall be independent of time. Under the assumption of the eigenfunctions being normalised to unity, the absolute square of those coefficients may be interpreted as the probability to find the system in the state $|\psi_k\rangle$. At time $t = 0$ the system gets perturbed and the Hamiltonian suddenly changes to H_1 . The time-independent Schrödinger equation then becomes:

$$H_1 \phi_n = E_n^{(1)} \phi_n \quad (3.5)$$

with the time-dependent solution being

$$\psi(t) = \sum_n c_n \phi_n e^{-iE_n^{(1)}t/\hbar} \quad (3.6)$$

again with a summation over the set of all eigenfunctions with time-independent coefficients c_n . Since the time-dependent Schrödinger equation is of first order in time, the wavefunction $\psi(t)$ must be continuous in time t . This continuity has to hold during the sudden change of the Hamiltonian as well. Thus at the time of the sudden change, $t=0$, the condition

$$\sum_k a_k |\psi_k\rangle = \sum_n c_n |\phi_n\rangle \quad (3.7)$$

has to hold. By multiplying this equation by $\langle \phi_n |$ and using $\langle \phi_n | \phi_m \rangle = \delta_{m,n}$ the time-independent coefficients c_n are given by:

$$c_n = \sum_k a_k \langle \phi_n | \psi_k \rangle \quad (3.8)$$

Under the assumption, that the Hamiltonian of the system changes instantaneously, this condition for the coefficients is exact. Since such a change usually happens during a time interval of finite length τ , the Hamiltonian H_0 first changes to H_i , with H_i being valid in the interval $0 < t < \tau$, and then, for $t > \tau$ to H_1 . The time-independent Schrödinger equation for the Hamiltonian H_i is then, as usual:

$$H_i \chi_l = E_l^{(i)} \chi_l \quad (3.9)$$

and the time-dependent solution $\psi(t) = \sum_l b_l \chi_l e^{-iE_l^{(i)}t/\hbar}$. Since the condition of the wavefunction remaining continuous during the perturbation still holds, at time $t=0$ the equation

$$\sum_k a_k \psi_k = \sum_l b_l \chi_l \quad (3.10)$$

holds, which yields the condition for the coefficients b_l :

$$b_l = \sum_k a_k \langle \chi_l | \psi_k \rangle \quad (3.11)$$

At the time $t = \tau$ the wavefunction has to stay continuous as well, thus yielding:

$$\sum_l b_l \chi_l e^{-iE_l^{(i)}\tau/\hbar} = \sum_n c_n \phi_n e^{-iE_n^{(1)}\tau/\hbar} \quad (3.12)$$

Plugging in the solution for the coefficients b_l from before, one gets for the c_n :

$$c_n = \sum_k \sum_l a_k \langle \phi_n | \chi_l \rangle \langle \chi_l | \psi_k \rangle e^{i(E_n^{(0)} - E_l^{(i)})\tau/\hbar} \quad (3.13)$$

For an instantaneous change of the system with $\tau = 0$ the above equation for the coefficients c_n gets the known form. For $\tau \neq 0$, the difference lies in the exponentials. If this time duration τ is small compared to $\frac{\hbar}{|E_n^{(0)} - E_l^{(i)}|}$, which means

$$\frac{(E_n^{(0)} - E_l^{(i)})\tau}{\hbar} \ll 1 \quad (3.14)$$

the change of the wavefunction in the interval $0 < t < \tau$ is small and can thus be neglected. The sudden approximation is then to set $\tau = 0$. In the following, the transition probability for the decay of a tritium nucleus in a tritium molecule will be derived using the Lippmann-Schwinger expansion. The total probability amplitude will be written as the sum of the zeroth, the first etc. order amplitudes with the zeroth order probability amplitude corresponding to the transition probability within the sudden approximation.

3.3 Derivation of the transition probability

The derivation of the transition probability is described in [4] and will be shown in detail now. Consider to start with the process



The Hamiltonian for the whole system $H = H_{i,f} + V_{i,f}$ is divided into the part $H_{i,f}$ describing the molecular system and a single lepton either in its initial or final state and $V_{i,f}$ describing the interaction between them. $H_{i,f}$ can be seen as the free Hamiltonian and $V_{i,f}$ as a small perturbation. The interaction term can be split in the following way:

$$V_{i,f} = U_{i,f} + W_{i,f} \quad (3.16)$$

Here $U_{i,f}$ stands for the coulombian interaction and $W_{i,f}$ for the weak interaction causing the decay. The transition probability of a molecule RT with a rest R to a molecule RHe^+ after beta-decay is described by:

$$|T_{fi}|^2 = |\langle f | W_i | i \rangle|^2 = |\langle \psi_f | W_i | \Phi_i \rangle|^2 \quad (3.17)$$

T_{fi} is the transition matrix element, $\langle \psi_f |$ is the final eigenstate of the Hamiltonian H and $|\Phi_i\rangle$ is the eigenstate of the free Hamiltonian H_i describing the initial motion of the RT molecule. W_i is the operator describing the weak interaction process. Now the final eigenstate $\langle \psi_f |$ of the Hamiltonian H can be expanded using the Lippmann-Schwinger ansatz:

$$\langle \psi_f | = \langle \Phi_f | + \langle \Phi_f | V_f (E - H_f + i\epsilon)^{-1} + \dots \quad (3.18)$$

where $(E - H_f + i\epsilon)^{-1}$ is the free Greens function and $\langle \Phi_f |$ is the eigenstate of the free Hamiltonian H_f . With $V_f = U_f$ the transition matrix element can be written in the following way:

$$T_{fi} = \langle \psi_f | W_i | \Phi_i \rangle = \langle \Phi_f | W_i | \Phi_i \rangle + \langle \Phi_f | U_f (E - H_f + i\epsilon)^{-1} W_i | \Phi_i \rangle + \dots = \quad (3.19)$$

$$\langle \Phi_f | W_i | \Phi_i \rangle + \langle \Phi_f | U_f (E - H_f + i\epsilon)^{-1} | \Phi_i \rangle + \dots = \quad (3.20)$$

$$T_{fi}^{(0)} + T_{fi}^{(1)} + \dots \quad (3.21)$$

Here $\Phi_{i,f}$ are the initial and final eigenvectors of the free Hamiltonian $H_{i,f}$. In the above equation higher order terms are neglected due to the smallness of the weak coupling constant. For the purposes of this work, only the zeroth order transition matrix element is of interest.

3.3.1 Evaluation of $T_{fi}^{(0)}$

The process

$$RT \rightarrow RHe^+ + e^- + \bar{\nu} \quad (3.22)$$

represents a decay of one particle into three final particles. According to field theory, such processes can be described as a scattering process. The emission of a particle corresponds to the absorption of an antiparticle with opposite energy. Thus the decay process can be described by a more symmetrical

$$RT + \nu \rightarrow RHe^+ + e \quad (3.23)$$

The free Hamiltonian for the initial state of the molecule can be written as

$$H_i = H_{RT} + H_\nu \quad (3.24)$$

whereas the free Hamiltonian for the final state is

$$H_f = H_{RHe^+} + H_\beta \quad (3.25)$$

The Hamiltonians can be further divided into

$$H_{f,i} = T^{c.m.} + H^{mol} + H^{nuc} \quad (3.26)$$

where $T^{c.m.}$ describes the center of mass motion of the molecule, H^{mol} describes the Coulombian Hamiltonian terms and H^{nuc} the internal motion of the nucleons. According to this, the wavefunctions of the initial and final states can be factorized in the following way:

$$\Phi_{f,i} = \psi_{f,i} \phi_l(\vec{r}_l) = \quad (3.27)$$

$$\frac{1}{(2\pi)^{\frac{3}{2}}} e^{i\vec{p}^f \cdot i\vec{r}} \psi_{nuc} \psi_{mol} \phi_l(\vec{r}_l) \quad (3.28)$$

The expression for the zeroth order transition matrix element then gets the form [4]

$$T_{fi}^{(0)} = \frac{1}{(2\pi)^3} \langle e^{i\vec{p}^f \vec{r}} \psi_{nuc}^f \psi_{mol}^f \phi_\beta(\vec{r}_l) | W_i | e^{i\vec{p}^i \vec{r}} \psi_{nuc}^i \psi_{mol}^i \phi_\nu(\vec{r}_l) \rangle$$

Evaluating this leads to

$$T_{fi}^{(0)} = \frac{1}{2\pi^6} \delta(\vec{K} - \vec{K}_c) T_{fi}^{weak(0)} T_{fi}^{(0)}(\vec{K}) \quad (3.29)$$

with K_C being the center of mass momentum and

$$T_{fi}^{(0)}(\vec{K}) = \langle \psi_f^{RHe^+} | e^{if_{AB} \vec{K} \vec{r}_{AB}} | \psi_0^{RT} \rangle \quad (3.30)$$

3.3.2 The zeroth order transition probability

The 0-th order transition probability can be written as [4]

$$|T_{fi}^{(0)}|^2 = \frac{1}{2\pi^6} \delta(\vec{K} - \vec{K}_c) |T_{fi}^{weak(0)}|^2 |T_{fi}^{(0)}(\vec{K})|^2 \quad (3.31)$$

If the transition probability is averaged over all directions of the neutrino, $|T_{fi}^{weak(0)}|$ can be assumed to be constant. So the only part of the above formula, that has to be evaluated, is $|T_{fi}^{(0)}(\vec{K})|^2$. The 0-th order transition amplitude can be written as:

$$T_{fi}^{(0)}(\vec{K}) = \langle \psi_f^{RHe^+} | e^{if_{AB} \vec{K} \vec{r}_{AB}} | \psi_0^{RT} \rangle \quad (3.32)$$

where ψ_0^{RT} is the wavefunction of the initial molecule containing a tritium atom T and some rest R, whereas $\psi_f^{RHe^+}$ is the wavefunction of the final molecule after beta-decay. $f_{AB} = \frac{m_B}{m_A + m_B + 2m_e}$ is a prefactor resulting from the calculation of the zeroth order transition matrix element. Working with the Born-Oppenheimer approximation, those wavefunctions can be written as $\psi_0^{RT} = \phi_0 \xi_{000}^0$ and $\psi_f^{RHe^+} = \phi_n \xi_{\nu J m_J}^n$, with ϕ_0 and ϕ_n being the initial and final electronic wavefunctions. ξ_{000}^0 and $\xi_{\nu J m_J}^n$ are the rovibrational initial and final wavefunction for a given electronic state n. To get the transition probability, one has to sum over all rovibrational states belonging to a final electronic state n.

$$|T_{ni}^{(0)}|^2 = \sum_{\nu, J, m_J} |\langle \psi_f^{RHe^+} | e^{if_{AB}\vec{K}\vec{r}_{AB}} | \psi_0^{RT} \rangle|^2 = \quad (3.33)$$

$$\sum_{\nu, J, m_J} \langle \psi_0^{RT} | e^{-if_{AB}\vec{K}\vec{r}_{AB}} | \psi_f^{RHe^+} \rangle \langle \psi_f^{RHe^+} | e^{if_{AB}\vec{K}\vec{r}_{AB}} | \psi_0^{RT} \rangle = \quad (3.34)$$

$$\sum_{\nu, J, m_J} \langle \phi_0 \xi_{000}^0 | e^{-if_{AB}\vec{K}\vec{r}_{AB}} | \phi_n \xi_{\nu J m_J}^n \rangle \langle \phi_n \xi_{\nu J m_J}^n | e^{if_{AB}\vec{K}\vec{r}_{AB}} | \phi_0 \xi_{000}^0 \rangle = \quad (3.35)$$

$$\sum_{\nu, J, m_J} \langle \xi_{000}^0 | \langle \phi_0 | e^{-if_{AB}\vec{K}\vec{r}_{AB}} | \phi_n \rangle | \xi_{\nu J m_J}^n \rangle \langle \xi_{\nu J m_J}^n | \langle \phi_n | e^{if_{AB}\vec{K}\vec{r}_{AB}} | \phi_0 \rangle | \xi_{000}^0 \rangle = \quad (3.36)$$

$$\langle \xi_{000}^0 | \langle \phi_0 | e^{-if_{AB}\vec{K}\vec{r}_{AB}} | \phi_n \rangle \langle \phi_n | e^{if_{AB}\vec{K}\vec{r}_{AB}} | \phi_0 \rangle | \xi_{000}^0 \rangle \sum_{\nu, J, m_J} | \xi_{\nu J m_J}^n \rangle \langle \xi_{\nu J m_J}^n | \quad (3.37)$$

According to orthonormality $\sum_{\nu, J, m_J} | \xi_{\nu J m_J}^n \rangle \langle \xi_{\nu J m_J}^n | = \mathbb{1}$. Since the integration in the inner brackets is not dependent on the vector \vec{r}_{AB} , one gets:

$$|T_{ni}^{(0)}|^2 = \langle \xi_{000}^0 | \langle \phi_0 | e^{-if_{AB}\vec{K}\vec{r}_{AB}} e^{if_{AB}\vec{K}\vec{r}_{AB}} | \phi_n \rangle \langle \phi_n | \phi_0 \rangle | \xi_{000}^0 \rangle = \quad (3.38)$$

$$\langle \xi_{000}^0 | \xi_{000}^0 \rangle | \langle \phi_n | \phi_0 \rangle|^2 \quad (3.39)$$

With the electronic overlap matrix element $S_{n0} = \langle \phi_n | \phi_0 \rangle$ one finally gets the following expression for the zeroth order transition probability:

$$|T_{ni}^{(0)}|^2 \approx |S_{n0}(R_e)|^2 \int_0^\infty |\xi_0|^2 dR = |S_{n0}(R_e)|^2$$

So one can conclude, that the overall probability for a molecule to be in a electronic state n after beta-decay is in a first approximation independent on the recoil momentum of the beta-electron and thus on its energy.

3.4 The Born-Oppenheimer Approximation

With the knowledge, how to calculate the matrix element, it is necessary to know the wavefunction of the initial and the final state. In order to calculate the initial

and final channel wavefunctions, the Schrödinger equation for both, the decaying and the daughter molecule, need to be solved. Therefore the Born-Oppenheimer approximation is used [9]. The molecular Schrödinger equation will be transformed into a system of coupled equations. After this, the position of the nuclei will be assumed to be fixed as seen from the electrons. In this case, relativistic as well as spin interactions are being seen as a small perturbation. Start with the general Hamilton operator for a molecule [11]

$$H = \sum_N \frac{P_N^2}{2m_N} + \sum_n \frac{P_n^2}{2m_e} + \frac{e^2}{4\pi\epsilon} \left(\frac{1}{2} \sum_{n,m} \frac{1}{d_{nm}} - \sum_{N,m} \frac{Z_N}{d_{nm}} + \frac{1}{2} \sum_{N,M} \frac{Z_N Z_M}{d_{NM}} \right) \quad (3.40)$$

Here, P is the momentum operator. The large indices indicate the nuclei whereas the small ones stand for the electrons. The distance between particles is given by $d_{nm} = |\vec{r}_n - \vec{r}_m|$. The term $\frac{1}{2} \sum_{n,m} \frac{1}{d_{nm}}$ describes the coulomb interaction between the electrons, $\sum_{N,m} \frac{Z_N}{d_{nm}}$ stands for the coulomb interaction between the nuclei and the electrons and $\frac{1}{2} \sum_{N,M} \frac{Z_N Z_M}{d_{NM}}$ describes the coulomb interaction between the nuclei themselves. Defining $T_K = \sum_N \frac{P_N^2}{2m_N}$, which describes the dynamics of the nuclei, the Hamiltonian can be rewritten as

$$H = H_0 + T_K \quad (3.41)$$

where H_0 is defined as the Hamilton operator describing the dynamics of the electrons as well as the coulomb interaction with the nuclei. The Schrödinger equation, which will be the goal to simplify, can then be written as:

$$(H_0 + T_K)\psi(\vec{R}, \vec{r}) = E\psi(\vec{R}, \vec{r}) \quad (3.42)$$

Here, \vec{R} is the internuclear separation. First, the position of the nuclei is assumed to be fixed. Thus, the above equation reduces to:

$$H_0\phi^{\vec{R}}(\vec{r}) = E^{(0)}(\vec{R})\phi^{\vec{R}}(\vec{r}) \quad (3.43)$$

This equation is called the electronic Schrödinger equation. The index \vec{R} indicates, that the wavefunction $\phi^{\vec{R}}(\vec{r})$ is still dependent on the internuclear separation. The solutions to this equation are the eigenstates $\phi_s^{\vec{R}}(\vec{r})$ together with the eigenvalues

$E_s^{(0)}(\vec{R})$. The above equation will be solved for each fixed internuclear separation. The corresponding eigenvalues are called potential curves. Using these potential curves, the wavefunction $\psi(\vec{R}, \vec{r})$, which solves the whole molecular Schrödinger equation, can be expanded in terms of the eigenstates $\phi_s^{\vec{R}}(\vec{r})$:

$$\psi(\vec{R}, \vec{r}) = \sum_s \chi_s(\vec{R}) \phi_s^{\vec{R}}(\vec{r}) \quad (3.44)$$

Here, the $\chi_s(\vec{R})$ are the coefficients, which only depend on the internuclear separation but not on the position of the electrons \vec{r} . Those coefficients can later be identified as the nuclear wave functions. This series can now be put into the Schrödinger equation.

$$\sum_s E_s^{(0)}(\vec{R}) \chi_s(\vec{R}) \phi_s^{\vec{R}}(\vec{r}) + \sum_s T_K(\chi_s(\vec{R}) \phi_s^{\vec{R}}(\vec{r})) = E \sum_s \chi_s(\vec{R}) \phi_s^{\vec{R}}(\vec{r}) \quad (3.45)$$

It was used, that the wavefunctions $\phi_s^{\vec{R}}(\vec{r})$ are eigenstates of the Hamiltonian H_0 . In the next step, the above equation will be averaged out over the wavefunctions of the electrons, aiming at getting an equation for the nuclear wavefunctions. Therefore, the equation will be multiplied from the left by $(\phi_t^{\vec{R}}(\vec{r}))^*$ and afterwards integrated over the position of the electrons \vec{r} . It will be used, that the wavefunctions $\phi_s^{\vec{R}}(\vec{r})$ are orthonormal, thus $\langle \phi_t^{\vec{R}}(\vec{r}), \phi_s^{\vec{R}}(\vec{r}) \rangle = \delta_{t,s}$.

$$E_t^{(0)} \chi_t(\vec{R}) + \int d\vec{r} (\phi_t^{\vec{R}}(\vec{r}))^* T_K \left(\sum_s \chi_s(\vec{R}) \phi_s^{\vec{R}}(\vec{r}) \right) = E \chi_t(\vec{R}) \quad (3.46)$$

The integral can be written as:

$$\int d\vec{r}(\phi_t^{\vec{R}}(\vec{r}))^* T_K \left(\sum_s \chi_s(\vec{R}) \phi_s^{\vec{R}}(\vec{r}) \right) = \quad (3.47)$$

$$\int d\vec{r}(\phi_t^{\vec{R}}(\vec{r}))^* T_K \left(\sum_s \chi_s(\vec{R}) \right) \phi_s^{\vec{R}}(\vec{r}) + \quad (3.48)$$

$$\int d\vec{r}(\phi_t^{\vec{R}}(\vec{r}))^* T_K \left(\sum_s \phi_s^{\vec{R}}(\vec{r}) \right) \chi_s(\vec{R}) + \quad (3.49)$$

$$\hbar^2 \int d\vec{r}(\phi_t^{\vec{R}}(\vec{r}))^* \sum_{s,k} \frac{1}{m_k} \partial_{\vec{R}_k} \phi_s^{\vec{R}}(\vec{r}) \partial_{\vec{R}_k} \chi_s(\vec{R}) \quad (3.50)$$

The first summand can be written as $T_K \chi_t(\vec{R})$. This can be used to implicitly define c_{ts} .

$$\int d\vec{r}(\phi_t^{\vec{R}}(\vec{r}))^* T_K \left(\sum_s \chi_s(\vec{R}) \phi_s^{\vec{R}}(\vec{r}) \right) = T_K \chi_t(\vec{R}) + \sum_s c_{ts} \chi_s(\vec{R}) \quad (3.51)$$

Using this, the molecular Schrödinger equation can be written as a system of equations:

$$H_0 \phi^{\vec{R}}(\vec{r}) = E^{(0)} \phi^{\vec{R}}(\vec{r}) \quad (3.52)$$

$$T_K \chi_t(\vec{R}) + \sum_s c_{ts} \chi_s(\vec{R}) = (E - E_t^{(0)}) \chi_t(\vec{R}) \quad (3.53)$$

As can be seen in the above equation, getting the nuclear wavefunctions requires the knowledge of the eigenvalues of the electronic equation for a fixed internuclear separation, thus the potential curves. It is not necessary to know the eigenstates of the electronic equation, to obtain the nuclear wavefunctions. To decouple this system, the interaction between the electron shell and the nuclear motion needs to be neglected. Therefore the Born-Oppenheimer approximation is given by:

$$c_{ts} = 0 \quad (3.54)$$

3.5 B-Splines

Since the Schrödinger equation, which is the equation needed to be solved to get the initial and final channel wavefunctions, can be solved analytically only in very few cases, B-Splines are one option used to solve it numerically, which will be used in this work. In this section, a brief introduction to the mathematics of B-Splines will be given. A complete introduction to their theory is given in [12]. Consider a one-dimensional box with coordinate x . A B-Spline basis set in this box with endpoints $x=a$ and $x=b$ has the following properties:

- A certain amount of interior points $s-1$ is being chosen, which divides the box into subintervals. The sequence of increasing points $s+1$ is called breakpoints. As an example, take the one-dimensional box $[0, 5]$ with $s=5$ subintervals. The breakpoint sequence then is $0, 1, 2, 3, 4, 5$
- The order k of the B-Splines describes the maximum degree $k-1$ of polynomial pieces, that the B-Splines are made of.

$$p(x) = a_{k-1}x^{k-1} + \dots + a_1x_1 + a_0 \quad (3.55)$$

- The last property are the so called knots, which are a sequence of points x_i . Every breakpoint is connected to one or more knots, which each knot having a multiplicity. The higher the multiplicity, the less continuous a function gets. In general the multiplicity is chosen to be the order of the B-Splines at the endpoints and unity for the interior points of the box. This yields, that that the number of knots for a given box and breakpoint sequence is equal to $s+2k-1$. For example, consider the above breakpoint sequence and an order of the B-Splines $k=4$. The obtained knot sequence then would be $x_i = 0, 0, 0, 0, 1, 2, 3, 4, 5, 5, 5, 5$ with a total number of 12 knots.

In the process of solving the Schrödinger equation using the above described Basis set, a box with a size r is chosen together with an order of B-Splines k_r . The knot sequence corresponding to the breakpoint sequence, r_i is constructed of n_r B-Splines. A solution for the wavefunction can then be approximated by the linear combination

$$\psi(r) = \sum_{\alpha=1}^{n_r} C_{\alpha} B_{\alpha}(r) \quad (3.56)$$

with C_α being the coefficients. Using this knowledge and the code written by Saenz to exactly calculate the FSD, a simplified model for an energy-dependence will be developed. In the next section, the four main parts of the whole final state probability distribution will be shortly described.

3.6 Description of the FSD

After the β -decay of a tritium atom being bound in a T_2 molecule, the final state energy distribution can be seen in Figure 3.1 [8].

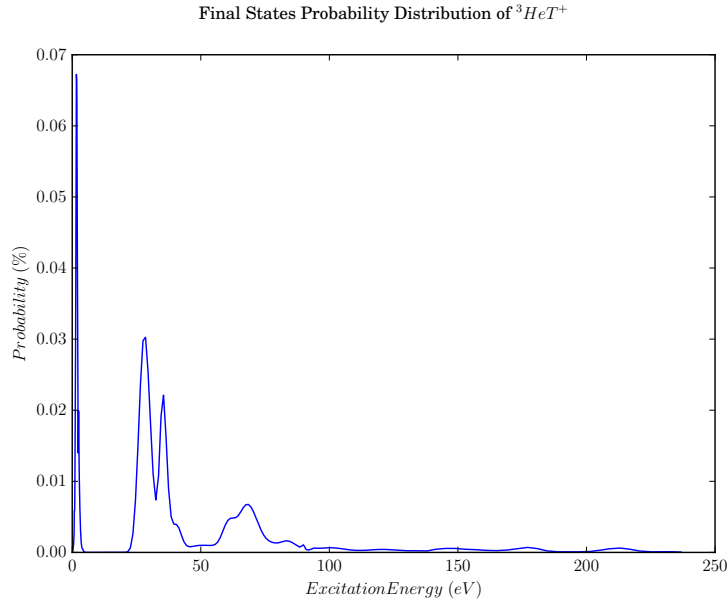


Figure 3.1: The whole final state distribution for a T_2 molecule as calculated in [8] for an endpoint energy of 18.6 keV

It can be divided into four main parts. The first narrow peak in the FSD describes the remaining electron energy distribution in the rovibrational broadened ground-state. The following two peaks stand for the first five electronically excited states, especially the two first excited states, that go up to an energy of $\approx 50\text{eV}$. After that follows the electronic continuum, that goes up to an energy of $\approx 240\text{eV}$. The FSD from 240 eV to higher energies can be described by an atomic tail. The

groundstate of the FSD can be, as explained in Robertson’s paper, described by a gaussian. The groundstate is broadened due to rotational and vibrational excitations and can, according to [1] be described with the formalism of an anharmonic quantum mechanical oscillator. The center of the gaussian lies around the recoil energy of the daughter molecule. After the beta decay the orbital electron can also end in an electronically excited state. The first five excited states are dissociative. The $n_f = 2, 4$ and 5 states dissociate into a He^+ ion plus an T atom. The other two states, $n=3$ and 6 dissociate into a He atom and a T^+ ion. The probabilities for those states, except for the first and the second electronically excited state, lie below 1% [9]. In the energy range above the energies of the first five electronically excited states takes the effect of the nuclear motion of the molecule into account [5]. According to [8] the FSD above 240 eV can be described to a good accuracy by the following energy-dependent expression

$$P(E) \approx 14.7 \left(\frac{8e^{-(4\arctan\kappa)/\kappa}}{\sqrt{1 - e^{-4\pi/\kappa}(1 + \kappa^2)^2}} \right)^2 \frac{dE}{eV} \quad (3.57)$$

with $\kappa = \sqrt{(E - 45eV)/13.606eV}$.

3.7 Simplified model for an energy-dependent FSD

In this section a simplified model for an energy-dependent final state distribution is derived. The main focus lies on the groundstate and the first five electronically excited states. The electronic continuum is for simplicity assumed to remain unchanged for lower β -energies. For energies above 240 eV an energy-dependent formula is given in [8].

3.7.1 Energy-dependent groundstate

In the following it will be described, how an energy-dependent final-state distribution of the groundstate for the molecular decay of T_2 -molecules might look like. As described in [1] the groundstate of the FSD, which is broadened by rotational and vibrational excitations, is centered around the recoil energy of the daughter molecule

$$E_{rec} = \frac{1}{2M_{ges}} \left((E_{tot}^2 - m_e^2) + 2 |\vec{p}_e| |\vec{p}_\nu| \cos(\theta) + (E_\nu^2 - m_\nu^2) \right) \quad (3.58)$$

with $E_{tot} = (E_{kin} + m_e)$ being the total energy of the beta-electron and $E_\nu = (E_{max} - E_{tot})$ where E_{max} is the maximal energy that the beta-particle can get. M_{ges} is the total mass of the daughter molecule, which is assumed to be six times the proton mass (differences between neutrons and protons are neglected as well as the binding energy). In Figure 3.2 the recoil energy dependent on the kinetic energy of the beta-electron can be seen for emission angles of $\theta = 0$ and $\theta = \pi$ between the electron and the anti-electron neutrino.

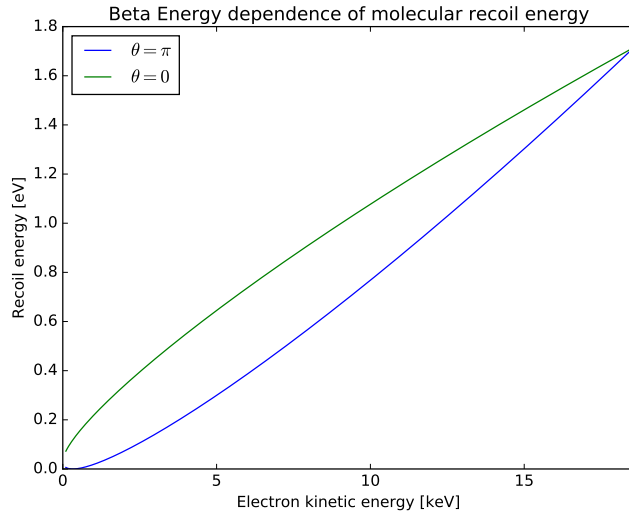


Figure 3.2: Recoil energy of the daughter molecule after beta-decay for $\theta = 0$ (green) and $\theta = \pi$ (blue) dependent on the kinetic energy of the beta-electron.

The broadening due to rovibrational excitations is described by a zero-point motion of a harmonic oscillator with a small anharmonic term. Its energy is given in [1] by:

$$E_{zp} = \frac{1}{2}\hbar\omega_c - a \left(\frac{1}{2}\hbar\omega_c \right)^2 \quad (3.59)$$

with $a = -0.0537(8) \text{ eV}^{-1}$ and $\hbar\omega_c = 0.5320(5) \text{ eV}$. The groundstate of the FSD can then be described by a gaussian distribution with standard deviation [1]

$$\sigma_{E_{exc}} = \sqrt{E_{rec} \cdot \frac{2\mu}{3M_T} E_{zp}} \quad (3.60)$$

Here, μ stands for the reduced mass of the system and M_T for the mass of the tritium atom. For lower electron energies one gets lower recoil energies of the daughter nucleus and the groundstate distribution will shift to smaller excitation energies. Due to the dependence of the standard deviation on the recoil energy, the distribution itself will get narrower for lower electron energies. This can be seen in Figure 3.3 for several kinetic energies.

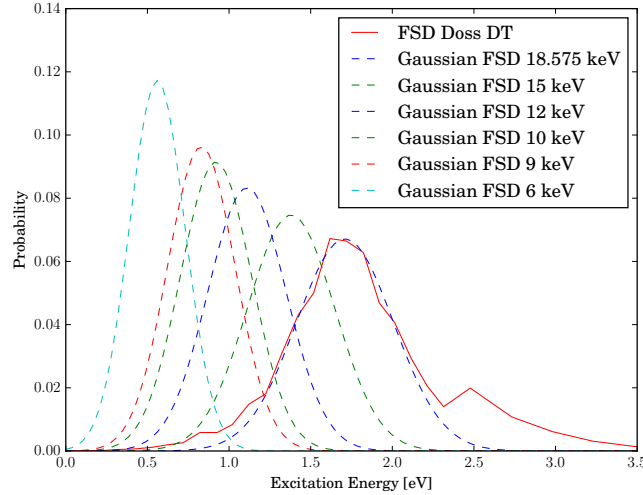


Figure 3.3: The groundstate FSD as calculated by Saenz (red solid curve). The normalisation of Gaussian groundstate (blue dashed curve) has been fitted to the calculated FSD, such that the two curves match. The only free parameter of the Gaussian distribution is the normalisation. The other curves describe how the groundstate distribution might change with lower beta-electron energies.

It was assumed for simplicity, that only emission angles of $\theta = \pi$ and $\theta = 0$ occur in this process with both being equally probable. This leads to a mean recoil energy of

$$E_{rec}^{mean} = \frac{(E_{tot}^2 - m_e^2) + (E_{max} - E_{tot})^2}{M_{ges}} \quad (3.61)$$

which gave the shift of the gaussian distribution to lower energies. The Gaussian groundstate distributions look quite different for different emission angles. This can be seen in Figure 3.4 for an angle of 0 , π and for the mean recoil energy shown in equation (4). However, this assumption is indeed justified. The probability of different emission angles is given by [10]

$$P(E, \theta)d\theta = A \cdot F(E, Z)(E + m_e)p(E_0 - E)^2 \cdot \left(1 + \alpha \frac{v}{c} \cos(\theta) + \frac{b}{E}\right) d\theta \quad (3.62)$$

Here α stands for the angular correlation coefficient, which can be calculated to be

$$\alpha = -0.1035 \quad (3.63)$$

This can be seen in Figure 3.5 as an example for a 6 keV, a 10 keV and a 15 keV beta-electron. In Figure 3.6 the angular probability distributions for those three beta-energies have been compared to an isotropic distribution with $P(\cos(\theta)) = \frac{1}{2}$. The assymetry of the distributions, which quantifies the deviation from an isotropic distribution and is given by [3]

$$A = \frac{P(\pi) - P(\pi/2)}{P(\pi/2)} \quad (3.64)$$

gets smaller for decreasing β -energies. For a 6 keV electron the asymmetry is around 1.57%, for a 10 keV electron 2.01% and for a 15 keV electron 2.45%. When calculating the recoil energy of the daughter molecule by weighting each energy by the probability of the angle occuring, the differences to the above assumed simplification are negligibly small. Thus the mean recoil energy can be written as:

$$E_{mean}^{rec} = \sum_{0 < \theta < 180} P(E, \theta) \cdot E_{rec}(E, \theta) \approx \frac{(E_{tot}^2 - m_e^2) + (E_{max} - E_{tot})^2}{M_{ges}} \quad (3.65)$$

So the energy dependence of the groundstate FSD can be described by a gaussian distribution, whose standard deviation is dependent on the recoil energy of the daughter molecule and thus on the recoil energy of the escaping β particle. The distribution gets shifted to lower recoil energies for lower β energies. The width of the distribution gets smaller and the normalization larger. This is in agreement with

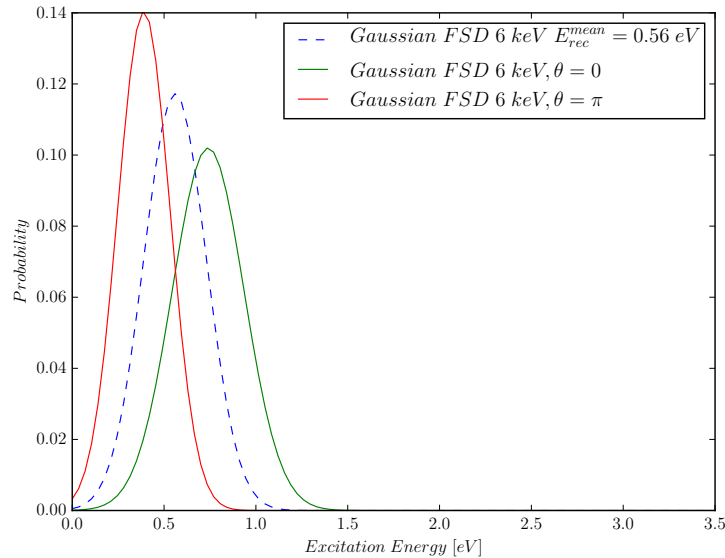


Figure 3.4: Gaussian Groundstate FSD for a 6 keV beta-particle with a scattering angle of $\theta = 0$ (green curve), $\theta = \pi$ (red curve) and an averaged recoil energy (blue dotted curve), where both scattering angles are assumed to occur equally often.

the fact, that the total probability for each electronically excited state (the sum over all rovibrational probabilities) is not dependent on the recoil energy (as described in the section about the derivation of the zeroth order transition probability). The used method works for electron energies between 6 keV and 18.5 keV. For lower energies, the gaussian distribution will imply probabilities for negative excitation energies, which is not wanted. It may be, that this is due to the fact, that interactions between the beta-particle and the daughter molecule can not be neglected for lower electron energies.

3.7.2 Energy-dependent excited FSD

In this section a simplified model for the energy-dependent behaviour of the FSD corresponding to the first five electronically excited states will be derived. It will be done in the following way: Since the FSD of the excited states is mainly influenced by the first and the second excited state, the focus will lie on them. Using the

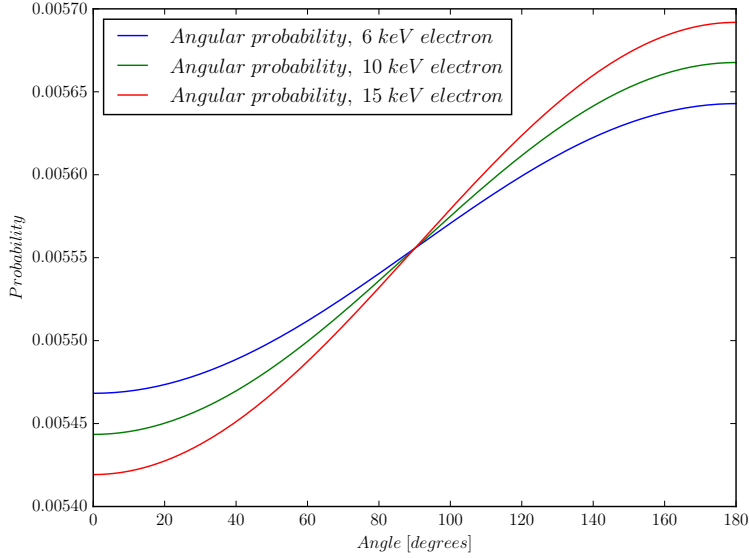


Figure 3.5: Angular probability distribution for a 6 keV (blue), a 10 keV (green) and a 15 keV (red) β^- particle.

calculation methods from Saenz et al. implemented in a FORTRAN code, the first task will be to reproduce the FSD for the first two excited states corresponding to an energy of the beta electron of 18.6 keV. The resulting FSDs will be gaussian like. In the next step, the same calculation methods are used to evaluate the FSDs for the first two excited states for lower energies of the escaping electron, i.e. 16,14 and 12 keV. They too will be gaussian like. Fitting gaussians to them and describing the three parameters height, width and mean value dependent on the beta energy will result in a gaussian model for the excited states FSD. The final state distribution for the excited bound states of the ${}^3\text{HeT}^+$ molecule includes the first five excited states $n_f = 2, 3, 4, 5, 6$. This can be seen in Figure 3.7. In an approximation this part of the FSD can be seen as the sum of two gaussian like distributions. The first gaussian is centered around an excitation energy of approximately 28 eV whereas the second one is centered around an energy of approximately 35 eV.

According to [9] starting with the tritium molecule in its total groundstate, i.e. the rotational J_i and vibrational ν_i quantum number being zero and the electronic quantum number $n_i = 1$, the total probabilities for the tritium molecule to end in an electronically excited state with quantum numbers $n_f = 2, 3, 4, 5, 6$ is shown in Table

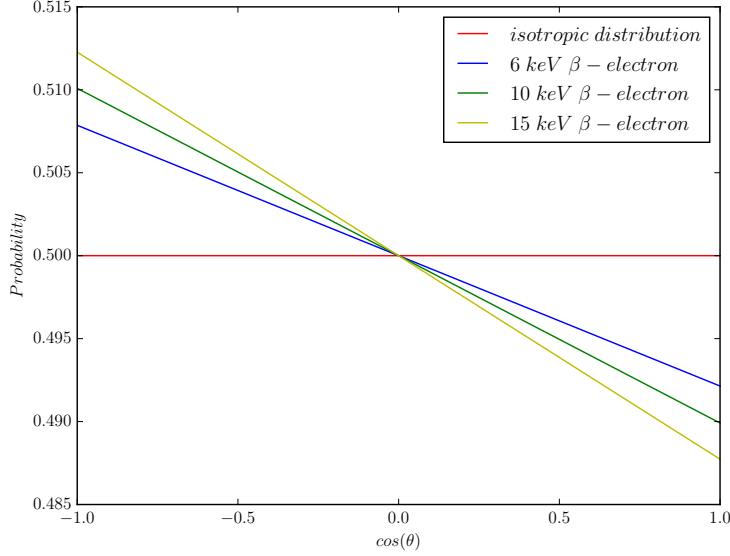


Figure 3.6: Angular probability distribution for a 6 keV (blue), a 10 keV (green) and a 15 keV (yellow) β -particle dependent on the $\cos(\theta)$ compared to an isotropic distribution (red) .

3.1. As can be seen, the probabilities for the states $n_f = 2$ sums up to 17.359 % and for $n_f = 3$ to 7.761 %. The probabilities for the electronic states $n_f = 4, 5, 6$ lie below 1%. Thus the first gaussian like part is mainly the first excited state, whereas the second gaussian like part is the probability distribution for the second excited state. In order to develop a simplified model for an energy-dependent description of the electronically excited FSD, the latter will be neglected. The procedure will be the following: First the FSD for each of the first two electronically excited states will be calculated separately for an endpoint energy of 18.6 keV using Saenz Code. This will be done to first reproduce old results and check, if the calculations run properly. In the next step, for each of those two excited states, the FSD will be calculated for β -electrons with an energy of 16,14 and 12 keV. To this distributions, gaussians will be fitted yielding a closed and simplified formula to describe the excited final state distribution dependent on the energy of the β -electron down to energies of 12 keV. To get the FSD for an electronically excited state n_f , the matrix element

$$\langle \psi_f | e^{i\vec{K}\vec{R}} | \psi_i \rangle \quad (3.66)$$

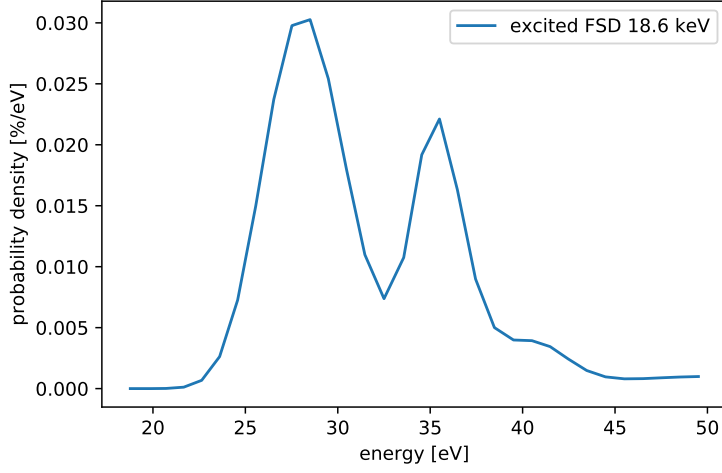


Figure 3.7: Final State probability distribution of the first five electronically excited states. The first gaussian like part of the distribution is mainly influenced by the first excited state whereas in the second gaussian like part the second excited states contributes.

| n | $P_n(J_i = 0)$ | Energy range [eV] |
|---|----------------|-------------------|
| 2 | 17.359 | 19.65 - 40.84 |
| 3 | 7.761 | 30.41 - 44.38 |
| 4 | 0.782 | 33.88 - 48.06 |
| 5 | 0.011 | 36.30 - 44.95 |
| 6 | 0.918 | 36.18 - 49.59 |

Table 3.1: Total probabilities for each electronically excited final state. The total probability for the states $n_f = 4, 5, 6$ is below one percent.

needs to be evaluated, with \vec{K} being the recoil of the β electron and \vec{R} the inter-nuclear separation. Therefore the channel wavefunctions $\psi_{i,f} = \psi_{n,J,\nu}$ have to be known. The initial state will be set to the total groundstate, i.e. $\psi_i = \psi_{n=1,J=0,\nu=0}$. The final channel wavefunctions will be $\psi_f = \psi_{n=2,J,\nu}$ and $\psi_f = \psi_{n=3,J,\nu}$. In the end, the FSD for an electronically excited state n_f will be

$$P_n = \sum_J |\langle \psi_{n,J,\nu} | e^{i\vec{K}\vec{R}} | \psi_{100} \rangle|^2 \quad (3.67)$$

summing over all rotational quantum numbers. The channel wavefunctions are calculated using the Born-Oppenheimer approximation. As can be seen in the section concerning the derivation of the zeroth order transition probability, the matrix element itself can be divided into an electronic overlap $\langle \phi_n | \phi_0 \rangle$ and the nuclear overlap. Using the nucfix code, the nuclear wavefunctions are calculated in the Born-Oppenheimer approximation using only the eigenvalues of the electronic Hamiltonian for a fixed internuclear separation, i.e. the potential curves. The actual electronic wavefunctions are not needed. The used potential curves for the initial and the final state were taken from [6] and can be seen in Figure 3.8 and Figure 3.9.

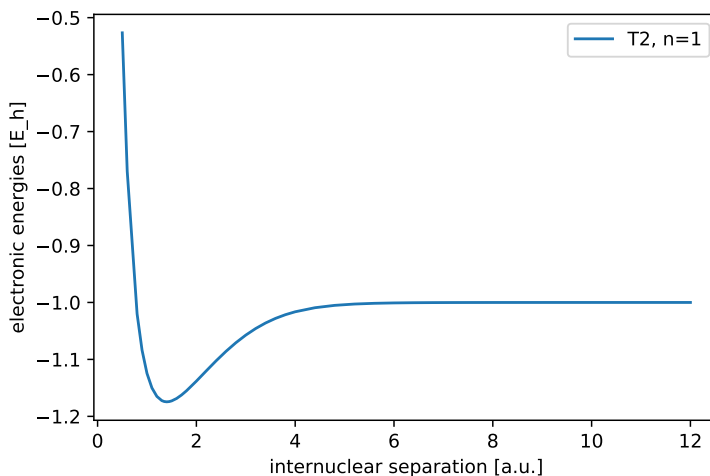


Figure 3.8: Potential curve for the electronic groundstate of the T_2 molecule. The electronic energies are shown in Hartree and the internuclear separation in atomic units (a.u.)

The nucfix code then calculates the nuclear wavefunctions numerically using a B-Spline Basis set. For the calculation of the initial and final channel wavefunction 602 B-Splines were used with a box radius of $R=30$. The order of the B-Splines was set to 10. With the knowledge of the nuclear wavefunctions, the transition probabilities to each electronically excited state are calculated using the rovib-trans code written by Saenz et.al. To do so, an appropriate number of rotational quantum numbers has to be chosen. Therefore the total probabilities of each rotational quantum number J , which is the sum over all vibrational quantum numbers ν

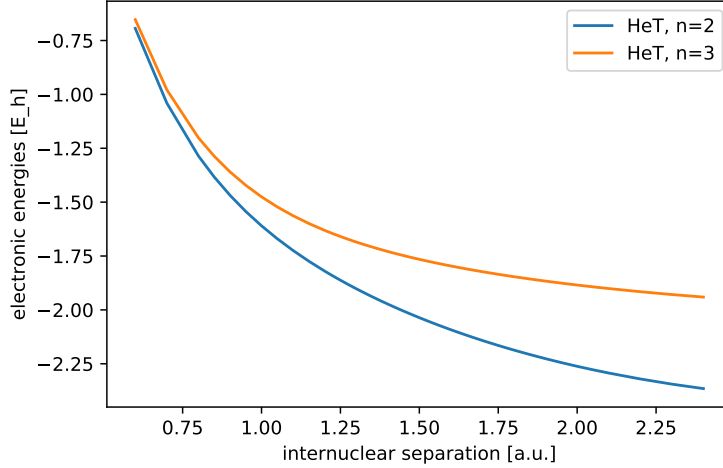


Figure 3.9: Potential curves for the first two electronically excited states of the ${}^3\text{HeT}^+$ molecule. The internuclear separation is shown in atomic units, the electronic energies in Hartree.

$$P_J = \sum_{\nu} P_{n,J,\nu} \quad (3.68)$$

is plotted in Figure 3.10.

As can be seen in Figure 3.10, the probability for rotational quantum numbers above 30 lies below 1%. Thus it is sufficient, to include only the first 30 J 's in the calculation of the transition probabilities:

$$P_n = \sum_{J=0}^{30} | \langle \psi_{n,J,\nu} | e^{i\vec{K}\vec{R}} | \psi_{100} \rangle |^2 \quad (3.69)$$

In the next step we get the final state distribution for each of the electronically excited states for an escaping β electron with an energy of 18.6 keV. The results can be seen in Figure 3.11 and Figure 3.12.

The plots in Figure 3.11 and Figure 3.12 of the distributions for each excited are in good agreement with earlier results. The distribution of the first excited state

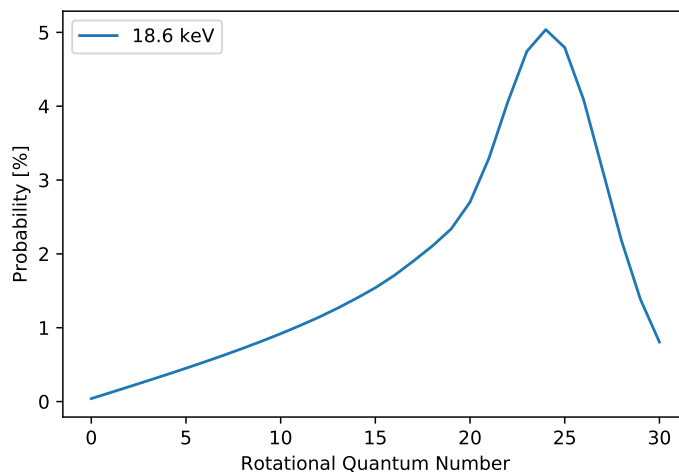


Figure 3.10: Probability distribution of the rotational quantum numbers J for an β electron energy of 18.6 keV. For each J the sum $P_{2J} = \sum_{\nu} P_{2,J,\nu}$ was evaluated. Since the probability for rotational quantum numbers above 30 is below 1%, it is sufficient to include only the first 30 in the calculation of the transition probability.

is centered around an energy of 28 eV, the distribution of the second excited state around 35.2 eV. The total probabilities sum up to 17.11% for the first excited state and to 7.67% for the second excited state. In the next step, the FSD for each of those excited states is evaluated at different, lower energies of the escaping β electron. First, it has to be known how high the number of rotational quantum numbers must be, in order to calculate the transition probability sufficiently. The J -distributions are plotted for different lower energies in Figure 3.13.

As can be seen in Figure 3.13, the probability distributions of the rotational states get shifted to lower J 's for smaller β energies. For the calculation of the 16 keV FSD, 30 rotational quantum numbers were used. For the calculation of the lower energy FSD's it is sufficient to include the first 25 rotational states in the evaluation. Doing so, the results of the low-energy FSD's for the first two electronically excited states are shown in Figure 3.14 and Figure 3.15.

The Final State Probability distributions for lower energies of the escaping β electron are shifted slightly to smaller excitation energies for both, the first and the second electronically excited state. The height of the distributions increases with decreasing

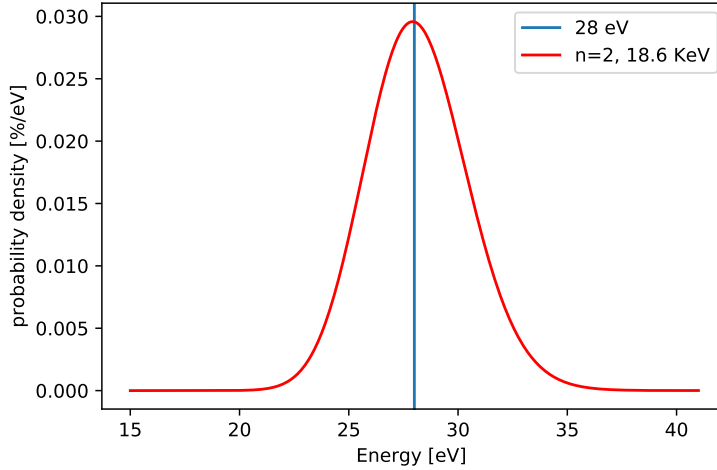


Figure 3.11: Final State Probability Distribution for the first electronically excited state $n=2$ corresponding to an β electron energy of 18.6 keV as calculated with the code of Saenz. The gaussian like distribution is centered around an excitation energy of 28 eV. The total probability sums up to $P_n = \sum_J P_{n,J,\nu} = 0.1711$

recoil energy for both FSD's, similarly to the behaviour of the groundstate FSD. A change in the width of the distributions cannot be seen with bare eyes. In the next step, it is assumed, that the FSD's for the electronically excited states can be approximated by gaussians, whose parameters now have to be evaluated dependent on the recoil energy of the escaping β particle. First, start with the first excited state distribution, $n=2$. A gaussian is fitted to each FSD corresponding to a certain recoil energy applying a least square fit. As an example, the gaussian fit to the first excited state distribution of a 18.6 keV electron is shown in Figure 3.16. The amplitude, center and width parameters for each energy are shown in Table 3.7.2

As can be seen in the Figures 3.17,3.18 and 3.19 showing the energy-dependent behaviour of the gaussian parameters, the amplitude increases with decreasing recoil energy whereas the the mean value decreases with decreasing recoil energy. The width of the gaussian decreases as well with decreasing recoil energy, besides a small deviation for 16 keV. To get an energy-dependent description of the FSD, the three parameters of the gaussian need to be described dependent on the β energy. Therefore, a linear fit is applied to all three of them. The plotted results can be seen in the figures below. In Table 3.7.2, the parameters slope and intercept are shown

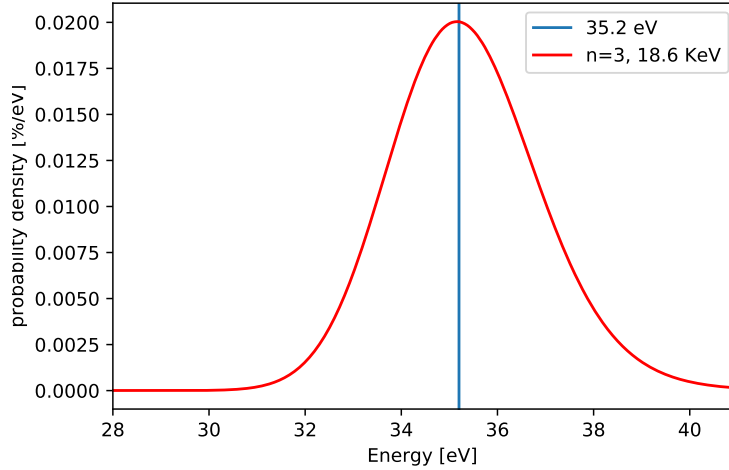


Figure 3.12: Final State Probability Distribution for the second electronically excited state $n=3$ corresponding to an β electron energy of 18.6 keV as calculated with the code of Saenz. The gaussian like distribution is centered around an excitation energy of 35.2 eV. The total probability sums up to $P_n = \sum_J P_{n,J,\nu} = 0.0.0767$

| Energy [keV] (n=2 gaussian) | Amplitude | Mean Value | Width |
|-----------------------------|------------|------------|------------|
| 18.6 | 0.02955441 | 28.0372802 | 10.6426924 |
| 16 | 0.02985940 | 27.5597441 | 10.6700508 |
| 14 | 0.03003489 | 27.2169073 | 10.5802247 |
| 12 | 0.03015821 | 26.8894655 | 10.3826095 |

Table 3.2: Parameters of the gaussians fitted to the FSD of the first electronically excited state for decreasing energies.

for those parameters.

The same method will now be applied to the second electronically excited state distribution. Again, a gaussian was fitted to each FSD corresponding to a certain recoil energy of the escaping electron. The fit to the 18.6 keV FSD of the $n=3$ state is shown in Figure 3.20. The three parameters, that came out of the fits, for different energies are shown in Table 3.7.2

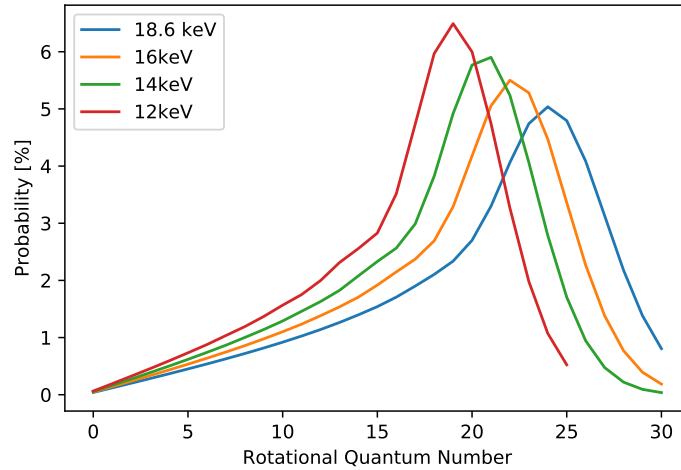


Figure 3.13: Probability distribution $P_{2J} = \sum_{\nu} P_{2,J,\nu}$ of rotational states J for β electron energies of 18.6, 16, 14 and 12 keV. For lower energies, the distributions get shifted to smaller rotational quantum numbers.

| Parameters (n=2 gaussian) | slope | intercept |
|---------------------------|-------------|------------|
| amplitude | -8.7767e-05 | 0.03125467 |
| mean value | 0.17406368 | 24.7884353 |
| width | 0.03830749 | 9.98864151 |

Table 3.3: Fit parameters slope and intercept for the linear fit of the amplitude, mean value and width of the gaussian corresponding to the FSD of the first electronically excited state.

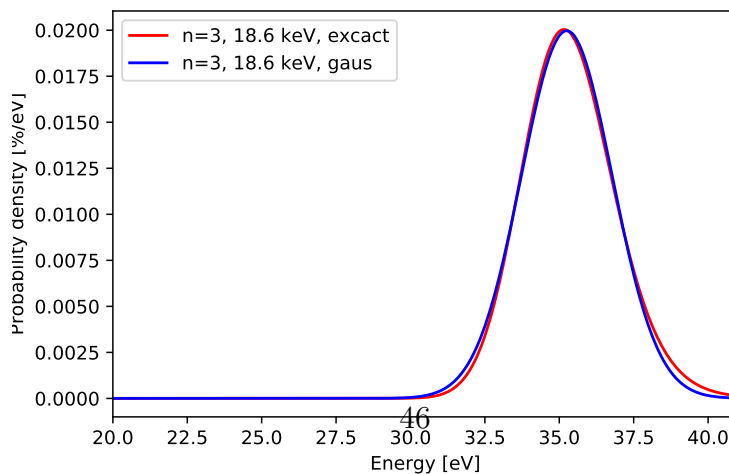


Figure 3.20: Final State Probability Distribution of the second electronically excited state together with a gaussian fit.

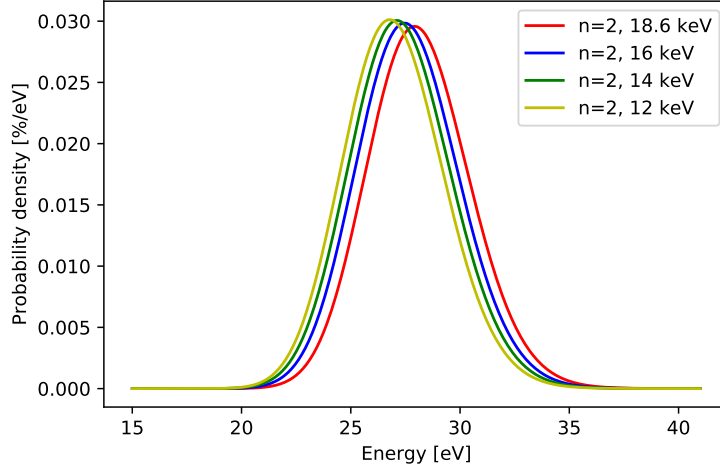


Figure 3.14: Final State Probability Distribution of the first excited state as calculated with the code of Saenz corresponding to β electron energies of 18.6, 16, 14 and 12 keV. The distributions get shifted slightly to lower excitation energies. The height of the FSD grows slightly for decreasing β energies.

| Energy [keV] (n=3 gaussian) | Amplitude | Mean Value | Width |
|-----------------------------|------------|------------|------------|
| 18.6 | 0.01996905 | 35.2513630 | 4.65029444 |
| 16 | 0.02031414 | 34.8725038 | 4.56251837 |
| 14 | 0.02039151 | 34.4781962 | 4.36190905 |
| 12 | 0.02031106 | 34.1726605 | 4.75174195 |

Table 3.4: Parameters amplitude, mean value and width of the gaussian fitted to the FSD of the second excited state.

The plotted parameters dependent on the recoil energy of the escaping electron for the second excited state are shown in Figures 3.21, 3.22 and 3.23 together with the best linear fits. It can be recognized, that the linear fit for the mean value worked fine. The amplitude and the width have been fitted linearly as well. The width does remains approximately constant in the linear fit. The parameters slope and intercept can be seen in Table 3.7.2.

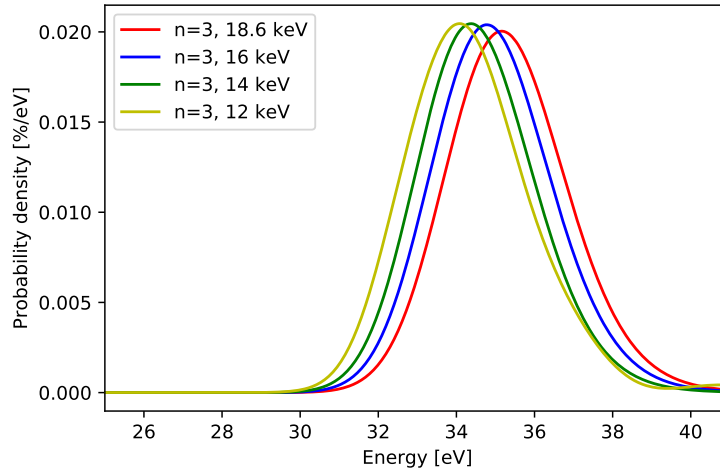


Figure 3.15: Final State Probability Distribution of the second excited state as calculated with the code of Saenz corresponding to β electron energies of 18.6, 16, 14 and 12 keV. The distributions get shifted slightly to lower excitation energies. The height of the FSD grows slightly for decreasing β energies.

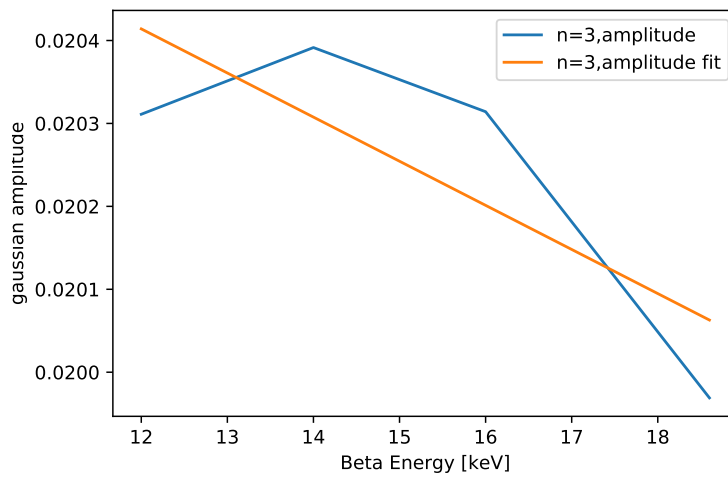


Figure 3.21: Amplitude of the gaussian distributions for the second excited state $n=3$ plotted vs the recoil energy of the escaping electron. A linear fit has been applied.

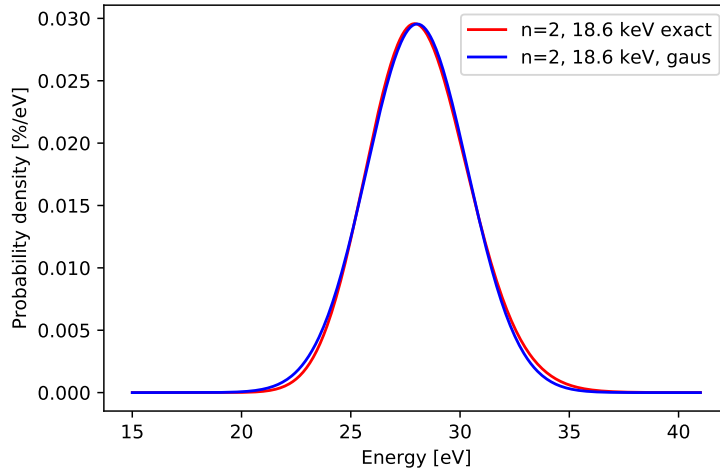


Figure 3.16: Final State Probability Distribution of the first electronically excited state $n=2$ for a 18.6 keV electron as calculated with the Code of Saenz and a gaussian fit to the distribution.

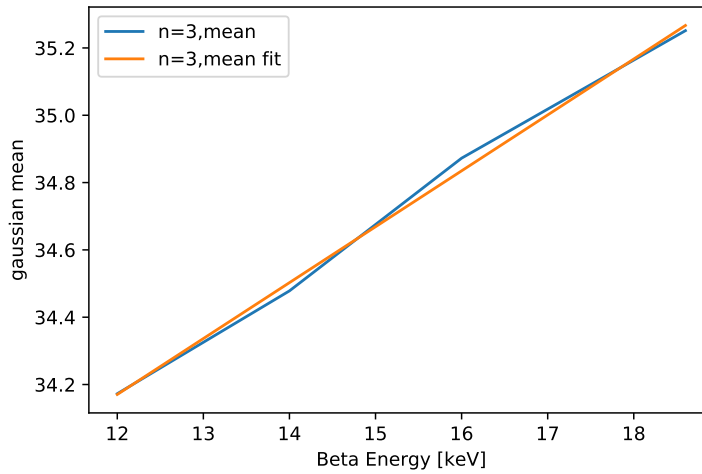


Figure 3.22: Mean Value of the gaussian distributions for the second excited state plotted against the recoil energy of the escaping electron. A linear fit has been applied.

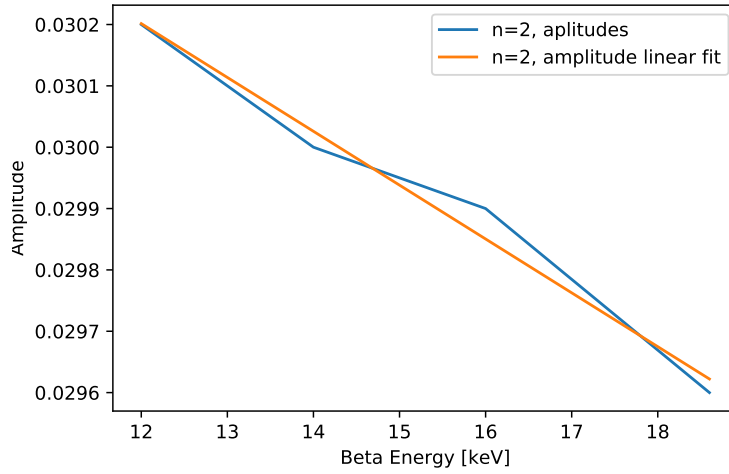


Figure 3.17: Amplitude of the Gaussian distribution for the first electronically excited state. Similarly to the behaviour of the energy-dependent groundstate FSD, the amplitude increases with decreasing recoil energy. A linear Fit was applied to this.

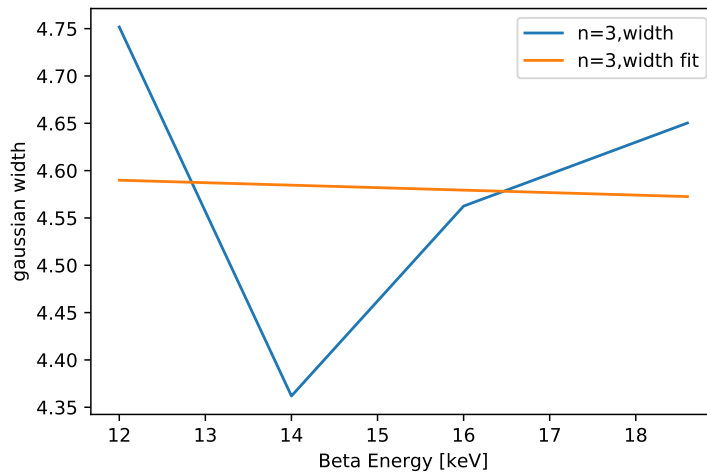


Figure 3.23: Width of the gaussian distributions dependent on the recoil energy of the escaping electron. A linear fit has been applied.

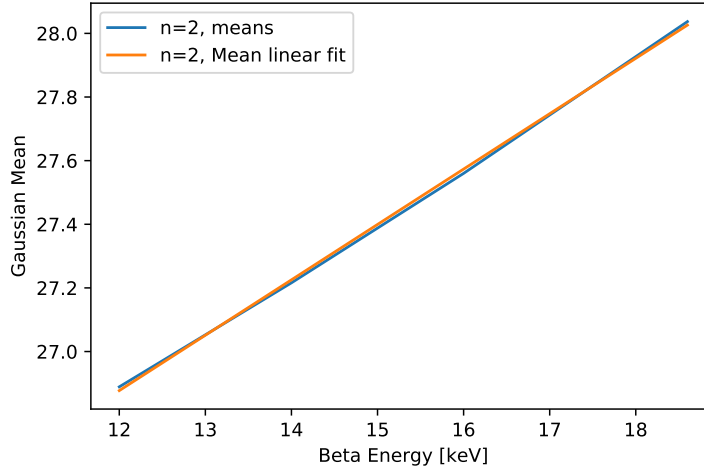


Figure 3.18: Mean of the Gaussian distribution for the first electronically excited state. Similarly to the behaviour of the energy-dependent groundstate FSD, the mean value of the gaussian decreases with decreasing recoil energy. A linear fit was applied.

| Parameters (n=3 gaussian) | slope | interscept |
|---------------------------|-------------|------------|
| amplitude | -5.3198e-05 | 0.02105239 |
| mean value | 0.16610911 | 32.1771279 |
| width | -0.00261947 | 4.62130099 |

Table 3.5: Parameters slope and interscept of the linear fits applied to the energy-dependent behaviour of the gaussian parameters corresponding to the second excited state FSD.

Together with this, a simplified way is found to describe the energy-dependence of the Final State Probability Distribution corresponding to the first five electronically excited states. The parameters are dependent on the recoil energy of the escaping electron yielding a gaussian for both the first and the second excited state. The sum of these two gaussians results in the Gaussian Excited FSD (GE-FSD) as can be seen in Figure 3.24

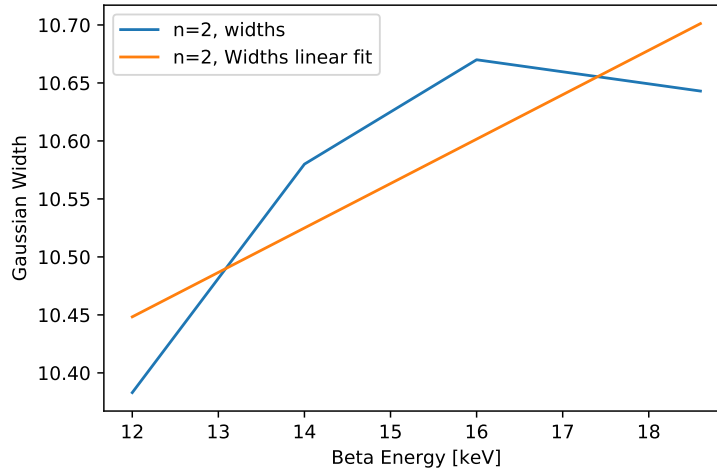


Figure 3.19: Width of the Gaussian distribution for the first electronically excited state. Similarly to the behaviour of the energy-dependent groundstate FSD, besides a small deviation for 16 keV, the width of the gaussian decreases with decreasing recoil energy. A linear fit was applied.

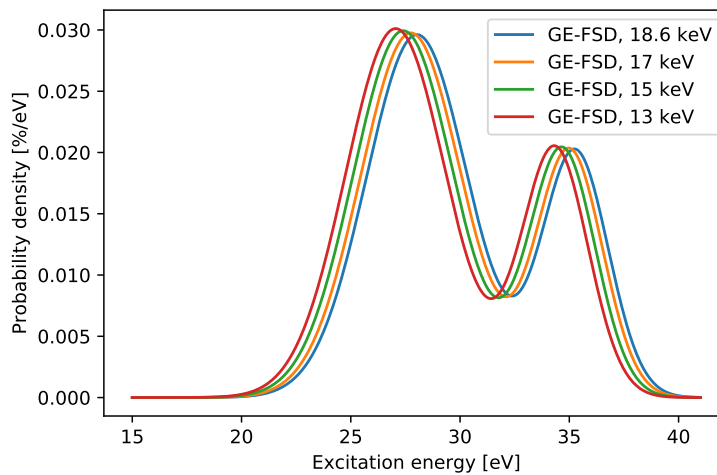


Figure 3.24: Gaussian Excited FSD (GE-FSD) for several energies below 18.6 keV. The whole distribution gets shifted slightly to lower excitation energies for decreasing recoil energy of the escaping electron as expected. As well an increase in the amplitude can be seen for decreasing recoil energy.

To see the differences between both FSDs, the absolute difference of the differential decay rates including energy-dependent FSD, which consists of the gaussian model for the groundstate and the first five excited states, an unchanged electronic continuum and the energy-dependent atomic tail, and the FSD calculated by Saenz

$$\Delta\Gamma = \left| \left(\frac{d\Gamma}{dE} \right)^{newFSD} - \left(\frac{d\Gamma}{dE} \right)^{DossFSD} \right| \quad (3.70)$$

are shown in Figure 3.25.

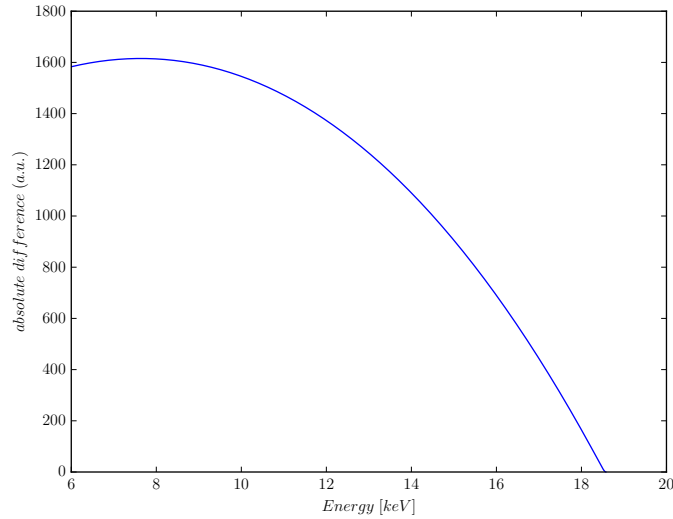


Figure 3.25: The absolute difference between the energy-dependent FSD beta-spectrum and the spectrum with final states calculated by Saenz. For electron energies near the endpoint the absolute difference goes to zero.

The absolute difference goes to zero for energies near the endpoint of the decay spectrum. This means, that the gaussian model of the FSD fits fine with the exactly calculated FSD. For lower energies, the difference increases. This is due to the fact, that the probability distribution shifts to lower energies in the gaussian case, whereas the exactly calculated remains.

Conclusion

A simplified model for an energy-dependent final state probability distribution corresponding to β energies down to 12 keV has been developed. The FSD itself is split into four parts: the groundstate, the first five electronically excited states, the continuum and the high energy range, which can be described by an energy-dependent atomic tail [8]. The electronic continuum has for simplicity been assumed to remain unchanged for decreasing energies. To get a model for the energy dependence of the groundstate, the method in [1] was used, which describes the rovibrational broadened groundstate of the FSD as a gaussian distribution with a standard deviation dependent on the zero-point motion of a slightly anharmonic oscillator and the recoil energy of the daughter molecule. For lower energies, the Gaussian distribution got shifted to lower excitation energies and got narrower due to the decreasing recoil energy. Taking the mean recoil energy (averaging over the angles $\theta = \pi$ and $\theta = 0$ and neglecting angles between) was a justified assumption, since the probability distribution for different emission angles is approximately uniform. To get an energy-dependent description for the excited FSD, the probability distributions for the first two electronically excited states have been calculated exactly for 18.6, 16, 14 and 12 keV using Saenz' Code. The evaluated distributions have been fitted by gaussians. The parameters amplitude, width and mean value have then been described dependent on the energy of the escaping electron yielding an energy-dependent description of the excited FSD down to 12 keV. Further work in this area would include developing a model for the electronic continuum as well as going down to lower energies and study the behaviour of the FSD.

Appendix

Calculation of the FSD using Saenz' Code

In order to calculate the Final State Probability Distribution for the first and second electronically excited state, two codes written by Saenz et al. in FORTRAN were used. The first code to use is the so called "nucfix" file. This code is used to calculate the nuclear wavefunction of both the initial and the final molecule in the decay process. In order to run it, at least four input parameters are required, optionally five. The first input parameter is the molecule, whose nuclear wavefunction will be calculated. The second argument is the B-Spline Basis set used to numerically solve the nuclear part of the Schrödinger equation (in the Born-Oppenheimer approximation). The content of the B-Spline input file can be seen in Figure 3.26 for the ${}^3\text{HeT}^+$ molecule.

The parameters given in this file are the masses of the atoms bound in the molecule, the range of rotational quantum numbers for which the nuclear Schrödinger equation needs to be solved and the properties of the B-Spline Basis set (box size, order, number of splines and knot sequence). The third argument is the electronic state, that the orbital electron should populate. Calculating the nuclear wavefunction for the initial tritium molecule, the electron was chosen to be in its total groundstate (electronic, rotational and vibrational groundstate). In the case of the daughter ${}^3\text{HeT}^+$ molecule, the first and the second electronically excited state were chosen. The fourth argument is the input file denoting the properties of the used potential curves.

As described in the section about the Born-Oppenheimer approximation, the nuclear part of the Schrödinger equation is dependent on the electronic eigenvalues - the potential curves. In this input file, the eigenvalues for different internuclear separations are specified. The fifth argument of the nucfix code is concerning either

```

*
*
*   Test input file for calculating electronic
*   wave functions using a B-spline basis:
*
*
*   Data concerning the molecular system:
*   -----
*
*   Masses m_A and m_B (or mu_{reduced} and -1.0D+00) : 1836.152D+00 7290.948D+00
*
*   Range of rotational quantum numbers J (begin, end) : 0 40
*
*   Electronic angular and spin momenta (projected on z): 0 0
*
*
*   Data concerning the B-spline basis:
*   -----
*
*   R_{max} (=box radius) : 30.00D+00
*
*   Order of the B-splines : 10
*
*   Number of B-splines : 602
*
*   Type of knot sequence : 0 ! 0: linear, 1: sine-like
*
*   First non-zero knot point: 1.0D-8 ! (Not used for linear knot sequence)
*
*
*   Data concerning the number of eigenvalues and -vectors to be stored:
*   -----
*
*   Save parameter : 2 ! 0: Do not store
*                   ! anything.
*                   ! 1: Store eigenvalues.
*                   ! 2: Store eigenvalues
*                   ! and -vectors.
*
*   Range of states to be stored (begin, end): 1 500 ! These parameters
*                                               ! are ignored, if
*                                               ! the save parameter
*                                               ! is set to 0.
*
*

```

Figure 3.26: The input file concerning the B-Spline Basis set used to numerically solve the nuclear part of the Schrödinger equation. The parameters given in this file are the masses of the atoms bound in the molecule, the number of rotational quantum numbers, for which the nuclear wavefunction needs to be calculated and the data concerning the B-Spline Basis set (box size, order, number of B-Splines and knot sequence).

the memory-optimized run of the code, the renormalization of the continuum wave functions or if the wavefunctions should be expanded on a finite radial grid.

Running the nucfix code for the initial and the final states molecules, one can proceed to the calculation of the transition probabilities using the so called "rovib_trans" file. To run this code, eleven arguments are needed. The first one is the file containing the eigenvalue and eigenstates of the initial molecule, as calculated before using the nucfix code. The second parameter is the B-Spline basis set file used to get the nuclear wavefunctions. The third parameter is the file containing the eigenvalue and eigenstate of the final molecule. In the fourth parameter, the input file of

the B-Spline Basis set corresponding to the final state molecule is given. The fifth parameter states the rotational quantum number of the initial molecule (which is chosen to be zero, since we want our initial molecule in its total groundstate). The sixth parameter denotes the vibrational state of the initial molecule, which is also set to zero. The 7th argument needed is the rotational quantum number of the final state molecule. The 8th parameter denotes the number of points used for coupling spline interpolations. In the 9th parameter, one is able to tell, if a continuum renormalization is needed, and if, for the initial, the final state or for both molecules. The 10th arguments is referring to the electronic overlap. As seen in the section about the derivation of the transition probability, the electronic wavefunctions are not needed to perform the calculation of the nuclear wavefunctions. The matrix element itself can be split into a matrix element for the nuclear wavefunctions and one for the electronic ones. The electronic overlaps have been calculated before. In the 11th parameter, one can state the recoil momentum of the beta electron in 1/a.u., where a.u. denotes atomic units. This allows us to perform the energy-dependent calculations of the Final State Probability Distribution. The output file resulting from that can be seen in Figure 3.27.

```

|-0.1331277413243D+01 -0.2499991989701D+01 0.2723354742162D-05 0.2016796159431E-031 0.8199179144749D-16 ( 0.44D-20) 0.2016796159431D-31 0
-0.1331260507830D+01 -0.2499975084288D+01 0.1962876702022D-04 0.8822411207833E-031 0.1714877178093D-15 ( 0.11D-19) 0.1883920736726D-30 1
-0.1331233660440D+01 -0.2499948236899D+01 0.4647615680309D-04 0.3741546158752E-030 -0.3531546478410D-15 ( 0.18D-19) 0.4825466895478D-30 2
-0.1331196547059D+01 -0.2499911123517D+01 0.8358953837995D-04 0.1309559355207E-029 -0.6606964394251D-15 ( 0.26D-19) 0.1792106044755D-29 3
-0.1331149095726D+01 -0.2499863672184D+01 0.1310408715716D-03 0.7138603001381E-031 -0.1542573931387D-15 ( 0.34D-19) 0.1863492074769D-29 4
-0.1331091325039D+01 -0.2499805901497D+01 0.1888115586195D-03 0.3108967095197E-033 -0.1017999196987D-16 ( 0.44D-19) 0.1863802971478D-29 5
-0.1331023287229D+01 -0.2499737863687D+01 0.2568493679799D-03 0.4365783670667E-030 -0.3814788622657D-15 ( 0.55D-19) 0.2308381338545D-29 6
-0.1330945046939D+01 -0.2499659623397D+01 0.3350896579493D-03 0.8776606557066E-030 0.5408821978048D-15 ( 0.67D-19) 0.3178041994252D-29 7
-0.1330856672185D+01 -0.2499571248563D+01 0.4234644921817D-03 0.429786556861E-033 -0.1196813346191D-16 ( 0.82D-19) 0.3178471782907D-29 8
-0.1330758229625D+01 -0.24994728068084D+01 0.5219069718976D-03 0.1100806617674E-031 -0.6057520443421D-16 ( 0.98D-19) 0.31894797699084D-29 9
-0.1330649783284D+01 -0.2499364359742D+01 0.6303533132268D-03 0.8250073776586E-031 -0.1658319809987D-15 ( 0.12D-18) 0.3271980506850D-29 10
-0.1330531392874D+01 -0.2499245969333D+01 0.7487437228972D-03 0.2103508107210E-030 -0.2647960288732D-15 ( 0.14D-18) 0.3482331317571D-29 11
-0.1330403113991D+01 -0.2499117690449D+01 0.8770226064061D-03 0.2021895009691E-030 0.2596083595014D-15 ( 0.16D-18) 0.3684520818540D-29 12
-0.1330264998180D+01 -0.2498979574639D+01 0.1015138416902D-02 0.2848080220034E-030 0.3081168728493D-15 ( 0.19D-18) 0.3969328840543D-29 13
-0.1330117093266D+01 -0.2498831669725D+01 0.1163043330901D-02 0.2923188145090E-032 -0.3121531752783D-16 ( 0.22D-18) 0.3972252028688D-29 14
-0.1329959443736D+01 -0.2498674020194D+01 0.1320692861263D-02 0.3465417360500E-031 -0.1074773985622D-15 ( 0.26D-18) 0.400690622294D-29 15
-0.1329792091128D+01 -0.2498506667586D+01 0.1488045469039D-02 0.7741359909574E-031 0.1606378941343D-15 ( 0.30D-18) 0.4084319801389D-29 16
-0.1329615074392D+01 -0.2498329650850D+01 0.1665062205042D-02 0.2177952559425E-030 0.2694409372153D-15 ( 0.34D-18) 0.4302115057332D-29 17
-0.1329428430204D+01 -0.2498143006662D+01 0.1851706393448D-02 0.1232359781432E-030 0.2026787097380D-15 ( 0.39D-18) 0.4425351035475D-29 18
-0.1329232193238D+01 -0.2497946769696D+01 0.2047943359514D-02 0.1706584608090E-031 -0.7542291004944D-16 ( 0.45D-18) 0.4442416881556D-29 19
-0.1329026396399D+01 -0.2497740972857D+01 0.2253740198282D-02 0.8262666716272E-030 -0.5254416147798D-15 ( 0.51D-18) 0.5270683553183D-29 20
-0.1328811071018D+01 -0.2497525647476D+01 0.2469065579133D-02 0.1056024021440E-029 -0.5933026269529D-15 ( 0.58D-18) 0.6326707574633D-29 21
-0.1328586247017D+01 -0.2497300823475D+01 0.2693889580558D-02 0.2686364648957E-030 -0.2992415216820D-15 ( 0.66D-18) 0.6595344039527D-29 22
-0.1328351953047D+01 -0.2497066529505D+01 0.2928183549951D-02 0.1061341712066E-030 -0.1880905555015D-15 ( 0.75D-18) 0.6701478210733D-29 23
-0.1328108216613D+01 -0.2496822793072D+01 0.3171919983888D-02 0.8222814989864E-031 -0.1655577944391D-15 ( 0.84D-18) 0.6783706360632D-29 24
-0.1327855064172D+01 -0.2496569640630D+01 0.3425072425177D-02 0.1356607600137E-030 -0.2126505427642D-15 ( 0.95D-18) 0.6919367120646D-29 25
-0.1327592521224D+01 -0.2496307097682D+01 0.3687615373643D-02 0.2408337280097E-030 -0.283335654958D-15 ( 0.11D-17) 0.7160200848655D-29 26
-0.1327320612389D+01 -0.2496035188847D+01 0.3959524208214D-02 0.6088548056893E-030 -0.4505015004375D-15 ( 0.12D-17) 0.7769055654345D-29 27
-0.1327039361479D+01 -0.2495753937937D+01 0.4240775118412D-02 0.1428500136296E-031 0.6900483404071D-16 ( 0.13D-17) 0.7783340655708D-29 28
-0.1326748791554D+01 -0.2495463368012D+01 0.4531345043690D-02 0.3276681409464E-030 0.3304885983643D-15 ( 0.15D-17) 0.8111008796654D-29 29

```

Figure 3.27: Part of the Output File of the rovb_trans code for the transition probability from the initial tritium molecule to the daughter molecule in its first electronically excited state with a rotational quantum number 0 corresponding to a 18.6 keV electron.

The important columns are the second and the fourth column. The second column denotes the excitation energy in Hartree with respect to the groundstate energy

of the ${}^3HeT^+$ molecule. The fourth column stands for the probability density. In order to produce a plot showing the Final States Probability Distribution of a certain electronically excited state as can be seen in the previous chapter, the excitation energies need to be converted to eV as well as the probability density from $\%$ /Hartree to $\%$ /eV. Additionally, the probability densities for the different final rotational quantum numbers need to be summed.

Bibliography

- [1] R.G.H. Robertson, 'Assesment of molecular effects on neutrino mass measurements from tritium beta decay'
- [2] S. Mertens, 'Sensitivity of next-generation tritium beta-decay experiments for keV-scale sterile neutrinos'
- [3] Herbert Daniel, Physik IV, Atome, Festkoerper, Kerne, Teilchen
- [4] Alejandro Saenz, Piotr Froehlich, Effect of final-state interactions in allowed β decays. I. General Formalism
- [5] Alejandro Saenz, Piotr Froehlich, Effect of final-state interactions in allowed β decays. II. Reliability of the β decay spectrum for T_2
- [6] Svante Jonsell, Alejandro Saenz, Piotr Froehlich, Neutrino-mass determination from tritium β decay: Corrections to and prospects of experimental verification of the final-state spectrum
- [7] Natasha Doss, Alejandro Saenz, Molecular effects in investigations of tritium molecule β decay endpoint experiments
- [8] Alejandro Saenz, Improved molecular final state distribution of HeT^+ for the β decay process of T_2
- [9] Natasha Doss, Calculated final state probability distributions for T2 beta-decay measurements
- [10] S.R. de Groot, On the theory of beta-radioactivity

- [11] C. David Sherrill, The Born-Oppenheimer Approximation
- [12] C. de Boor: A Practical Guide to Splines (Springer, New York, 1978) W. Pauli Scientific correspondence with Bohr, Einstein, Heisenberg
- [13] W. Pauli Scientific correspondence with Bohr, Einstein, Heisenberg
- [14] E. Fermi "Versuch einer Theorie der Beta-Strahlen I"
- [15] C.L. Cowan et. al. "Detection of the free neutrino: a confirmation"
- [16] B. Pontecorvo. "Mesonium and anti-mesonium"
- [17] G. Drexlin, V. Hannen, S. Mertens, and C. Weinheimer. Current Direct Neutrino Mass Experiments. Adv. High Energy Phys. 2013, 293986 (2013)
- [18] N. Severijns, M. Beck, and O. Naviliat-Cuncic, Tests of the standard electroweak model in nuclear beta decay, Reviews of Modern Physics, vol. 78, no. 3, pp. 991-1040, 2006
- [19] KATRIN Collaboration. KATRIN Design Report 2004. FZKA Scientific Report 7090, 2005.
- [20] C. Giunti and C. W. Kim. Fundamentals of Neutrino Physics and Astrophysics. Oxford University Press. 2007
- [21] M. Zbořil, S. Bauer, M. Beck, et al. "Ultra-stable implanted $^{83}\text{Rb}/^{83\text{m}}\text{Kr}$ electron sources for the energy scale monitoring in the KATRIN experiment".
- [22] B. Flatt and J. Wolf. "Design of the KATRIN pre-spectrometer". In: Nuclear Physics B - Proceedings Supplements 118 (2003), p. 483. issn: 0920-5632. doi: 10.1016/S0920-5632(03)01373-2.
- [23] K. Dolde. "Detector and read-out development to search for sterile neutrinos with KATRIN". MA thesis. Karlsruher Instituts für Technologie, 2016.

- [24] eV and keV sterile neutrino studies with KATRIN Master Thesis of Marc Korzeczek